AUGMENTED REALITY GUIDANCE FOR THE SURGICAL LOCALISATION OF PAEDIATRIC CHEST WALL TUMOURS

Rémi van der Woude

Master Thesis
Technical Medicine
September 2023

Augmented Reality Guidance for the Surgical Localisation of Paediatric Chest Wall Tumours

by

Rémi van der Woude

UNIVERSITY OF TWENTE.

A master's thesis
Submitted to the Faculty of Science and Technology
University of Twente
In partial fulfilment of the requirements
for the degree of Master of Science

in

Technical Medicine
Track Imaging and Interventions

September 7th, 2023

Graduation Committee

Chairman

Prof. dr. J.J. Fütterer

Department of Medical Imaging
Radboud University Medical Center
Nijmegen, The Netherlands

Robotics and Mechatronics
University of Twente
Enschede, The Netherlands

Medical supervisors

Prof. dr. M.H.W.A. Wijnen

Dr. A.F.W. van der Steeg

Department of Pediatric Surgery
Princess Máxima Center for Pediatric Oncology
Utrecht, The Netherlands

Technical supervisor

Dr. F.J. Siepel

Robotics and Mechatronics
University of Twente
Enschede, The Netherlands

Process supervisor

Drs. J. de Witte

Faculty of Science and Technology
University of Twente
Enschede, The Netherlands

Daily supervisor

M. Fitski, MSc

Department of Pediatric Surgery
Princess Máxima Center for Pediatric Oncology
Utrecht, The Netherlands

External member

J.K. van Zandwijk, MSc

Faculty of Science and Technology
University of Twente
Enschede, The Netherlands

Acknowledgements

Met het inleveren van deze thesis komt mijn afstudeerstage, en daarmee mijn opleiding tot technisch geneeskundige tot zijn eind. Met heel veel plezier kijk ik terug op de afgelopen zeven jaar waarin ik enorm veel heb geleerd en gedaan. Mijn afstudeerstage in het Prinses Máxima Centrum was voor mij de perfecte afsluiting. Tijdens de afgelopen elf maanden heb ik enorm veel geleerd op technisch vlak en kunnen ontdekken hoe leuk de wereld van software development is. Daarnaast heb ik me ook echt verder kunnen ontwikkelen tot technisch geneeskundige door samen met de chirurgen de HoloLens te implementeren tijdens alle borstwandresecties die het afgelopen jaar in het Máxima plaatsvonden. Hoewel ik de HoloLens op sommige momenten wel uit het raam kon gooien, had ik het voor geen goud willen missen.

Natuurlijk had deze thesis niet tot stand kunnen komen zonder de hulp en begeleiding van een heleboel personen. Allereerst wil ik beginnen met mijn medisch begeleiders, Marc Wijnen en Lideke van der Steeg. Ik ben enorm dankbaar dat jullie mij de mogelijkheid gaven om dit afstudeeronderzoek bij jullie te kunnen doen. Ik wil jullie bedanken voor de vrijheid en het vertrouwen dat jullie mij het afgelopen jaar hebben gegeven om samen met Augmedit tot een heel mooi eindproduct te komen. Ik heb heel veel geleerd van jullie academische kennis en kritische blik, en heb veel waardering voor jullie enthousiasme en informele begeleiding tijdens alle research meetings en sparsessies. Ten tweede wil ik Matthijs Fitski bedanken voor de ontzettend fijne dagelijkse begeleiding, ook tijdens mijn M2 stage. Ik wil je enorm bedanken voor je betrokkenheid, feedback en eindeloze goede ideeën tijdens het afgelopen jaar. Ik vond het heel fijn hoe je me volledig mijn eigen ding liet doen maar ook meteen klaarstond als ik ergens hulp bij nodig had. Alle TG-studenten hebben maar geluk met zo'n begeleider! Verder wil ik Françoise Siepel bedanken voor de technische begeleiding vanuit de UT. Ik kon het erg waarderen hoe je, ondanks onze weinige meetings, toch altijd op de hoogte was, de wetenschappelijke meerwaarde van mijn onderzoek bewaakte en altijd punten wist aan te stippen waar ik zelf nog helemaal niet aan had gedacht. Ik wil Jeroen de Witte bedanken voor mijn procesbegeleiding tijdens de afgelopen twee jaar. Als nuchtere Fries moest ik eerst niks van de intervisiesessies hebben, maar je hebt me toch weten te overtuigen. Jouw intervisiesessies hebben mij geleerd om stil te staan bij mijn ontwikkeling tot technisch geneeskundige en gemotiveerd om het beste uit mezelf te halen. Natuurlijk wil ik ook Jene Meulstee, Lucy Knöps en Milan Wijnmaalen bedanken voor de leuke samenwerking met Augmedit. Ik heb erg genoten van onze gezellige, maar toch professionele meetings. Door jullie enthousiasme was ik altijd weer enorm gemotiveerd om verder te gaan met mijn opdracht. Zonder jullie was dit onderzoek natuurlijk nooit gelukt, en ik wil jullie dan ook heel erg bedanken voor alle tijd en moeite die hierin is gestoken. Dit onderzoek was ook nooit tot stand gekomen zonder het eindeloze geduld van de chirurgen van het Máxima: Kees, Caroline en Guus. Ik wil jullie heel erg bedanken voor het vertrouwen en support tijdens de HoloLens OK's en de hulp tijdens de kadaverstudie. Zonder jullie was deze thesis maar voor de helft gevuld geweest. Daarnaast wil ik natuurlijk ook nog alle fijne collega's van de Wijnen onderzoeksgroep bedanken, met name de harde kern: Ceder, Matthijs, Myrthe, Dominique, Kevin, Jasper en Rixt. Deze onderzoeksgroep voelde als een warm bad en ik heb zoveel leuke herinneringen aan Barcelona, de research retreat, Winterberg, alle karaokesessies, vrimibo's en koffiepauzes. Ik heb enorm met jullie gelachen en wil jullie heel erg bedanken voor de gezellige tijd in het Máxima, ik ga het missen!

Ten slotte wil ik mijn lieve vrienden en familie bedanken voor het luisteren naar al mijn verhalen, twijfels, successen, maar ook geklaag tijdens mijn gehele studieperiode. Ik mag in mijn handjes knijpen met zoveel lieve mensen om me heen.

Nogmaals bedankt aan iedereen en veel leesplezier!

Rémi van der Woude

Utrecht, Augustus 2023

Abstract

Purpose

The surgical management of paediatric chest wall tumours is complex. Due to neoadjuvant chemotherapy, these tumours have often shrunk and become invisible and nonpalpable from the outside. During resection, surgeons therefore use multiple intraoperative imaging techniques such as thoracoscopy, ultrasonography, radiography, and fluoroscopy to locate the affected ribs and tumour. Intraoperative tumour localisation is hence a difficult and time-consuming process which has even led to the resection of incorrect ribs in the past.

The use of Augmented Reality (AR) could facilitate intraoperative tumour localisation and surgical decision making by allowing a direct projection of relevant anatomy onto the patient in the OR. A recent in-house study by Spijkerboer et al. (2022) has introduced an AR system to use the HoloLens 2 for tumour localisation prior to incision. Although the first results are promising, in-house experiences have shown that the system's landmark-based registration method is prone to user-dependent errors and registration inaccuracies. This thesis therefore explores the feasibility of surface matching as a new registration method to improve the conventional AR system.

Methods

Within this thesis, two surface acquisition methods were considered. The first method uses a tracked 3D printed pointer which is traced along the contour of the patient's thorax. The second method makes use of the Time-of-Flight (ToF) camera of the HoloLens 2.

First, a phantom study was performed to compare the registration accuracies of both surface matching methods to the conventional landmark-based registration method. Second, the clinical applicability of the surface matching methods was investigated through a cadaver study in which surgeons performed a simulated chest wall resection.

Results

The phantom study showed that with both surface matching methods it was possible to locate targets with an accuracy below 1 cm. When testing the methods in a surgical setting, the cadaver study proved that surgeons were able to locate the correct ribs with both surface matching methods. However, the contour registration method resulted in the most consistent and accurate projections. Additionally, unlike ToF camera registration, it was possible to perform registration on the post-incision surface of the exposed ribs with use of the contour registration method.

Conclusion

This thesis proved the feasibility of surface matching as a new registration method to use AR for intraoperative tumour localisation during paediatric chest wall resections. The contour registration method showed the most potential for both pre- and post-incision registration. Future studies should focus on testing the method in an even more realistic setting and improving the robustness and user-friendliness of the HoloLens application. Furthermore, efforts should be made to increase the willingness of surgeons to use the HoloLens during surgery. Ultimately, the use of AR could circumvent the need of additional imaging techniques and thereby facilitate intraoperative tumour localisation and surgical decision making during paediatric chest wall resections.

Table of Contents

List of Figures

List of tables

List of Abbreviations

AHAT	Articulated hand tracking
API	Application programming interface
AR	Augmented Reality
BuMel	Busulfan-melphalan
CT	Computed tomography
EM	Electromagnetic
ES	Ewing sarcoma
HDT	High dose chemotherapy
HMD	Head-mounted display
ICP	Iterative closest point
IE	Ifosfamide, etoposide
IR	Infrared
MRI	Magnetic resonance imaging
OR	Operation room
OS	Overall survival
PET	Positron emission tomography
PLA	Polylactic acid
QoL	Quality of life
QR	Quick response
RMS	Root mean square
SVD	Singular value decomposition
TCP	Transmission control protocol
ToF	Time-of-Flight
TRE	Target registration error
TreoMel	Treosulfan-melphalan
VDC	Vincristine, doxorubicin, cyclophosphamide

Introduction

Ewing sarcoma (ES) is a rare malignant bone tumour that is mainly found in children and adolescents, with two thirds of the patients being younger than 20 years[1,2]. In the Netherlands, around 13 children are diagnosed with ES every year[3]. ES mainly occurs in the tubular bones of the extremities, pelvic bones or the chest wall, but it can be found in almost any bone or soft tissue [2,4,5]. ES is a high-risk tumour and around 25% of patients present with metastasis at the time of diagnosis[4,6–8]. As metastatic disease at diagnosis is associated with a poor prognostic outcome, the overall 5-year survival rate of paediatric patients is solely 60-70%[9,10].

The aggressive behaviour of ES requires extensive treatment which usually consists out of neoadjuvant chemotherapy, radiation therapy and tumour resection, depending on the location and extend of the disease[4,8,9]. In the case of ES of the ribs, induction chemotherapy is followed by a chest wall resection. Due to the highly malignant nature of ES, the main goal of surgery is to achieve wide tumour resection margins.[6,11–13] This often means that the affected rib is removed together with adjacent ribs, leaving a chest wall defect that can cause significant deformities, such as scoliosis[12,14]. These chest wall resections require accurate tumour localisation and preoperative planning to achieve the most optimal outcome for the patient while still maintaining safe tumour margins. However, for ES of the ribs, intraoperative tumour localisation can be extremely difficult. These tumours tend to grow more inward into the pleural cavity and are therefore usually not visible from the outside. Secondly, due to neo-adjuvant chemotherapy, the tumour has often shrunk enormously and has also become non-palpable.[15,16] Intraoperative localisation of the affected rib is hence a time-consuming and complex process that requires multiple imaging modalities, depending on the tumour's extend, depth and position[15]. Surgeons generally use a combination of the preoperative CT and MR images, as well as intraoperative imaging techniques such as ultrasonography, thoracoscopy or fluoroscopy to localize affected rib and tumour and plan the resection. The used techniques differ per patient and thus no generalized approach for tumour localisation yet exists.[15,17]

A visualisation technique that could be a solution to these challenges is Augmented Reality (AR). AR enables the 3D visualisation of a virtual model within the real world, e.g. the operation room (OR). AR has the advantage of being a non-invasive visualisation technique that can give a direct impression of the patient's anatomy in 3D. When used with a head-mounted display (HMD), e.g. the HoloLens (Microsoft Corporation, Redmond, WA, USA), the virtual model can be displayed as a hologram and projected directly on the patient in the working field of the surgeon. This enables a more intuitive interpretation of the patient's anatomy. Furthermore, surgeons can limit their focus to the working field and do not have to switch between 2D monitors displaying the preoperative images and the intraoperative situation (the switching focus problem).[18–21]

Several studies have shown that AR already has great potential in many surgical fields such as orthopaedics, maxillofacial surgery or neurosurgery.[21–26] A recent in-house study by Spijkerboer et al. (2022) has explored the feasibility of AR in paediatric surgical oncology[27]. The HoloLens 2 was used to intraoperatively localize Ewing sarcoma of the ribs in paediatric patients prior to chest wall resection by projecting a virtual 3D model onto the patient. To align the virtual 3D model with the real position of the patient in the OR, a registration procedure is required. The system proposed by Spijkerboer et al. uses a common five-point registration method based on anatomical landmarks. During this registration procedure, the most optimal transformation is found between five recognizable landmarks derived from preoperative CT images, and the corresponding landmarks

on the patient in the OR. The surgeon therefore pinpointed five recognizable landmarks on the patient's skin, e.g. the nipple, birthmarks or scars with a surgical pointer. A Quick response (QR) code was attached to the pointer to allow the HoloLens to track the position of the pointer, and therefore save the intraoperative position of the five landmarks. Subsequently, a Procrustes algorithm was used to find the most accurate transformation between the position of the intraoperative landmarks and the corresponding landmarks in the preoperative CT scan. This transformation was then applied to the virtual 3D model to project the ribs and tumour onto the patient in the OR. A second reference QR code was attached to the patient to adjust for respiratory movement and enable a stable visualisation. The proposed system has the potential to enable intraoperative 3D visualisation and tumour localisation, hereby facilitating surgical planning and management of chest wall resections. However, there are still improvements to be made in order to realize actual implementation in clinical practice.

Firstly, the thorax generally lacks the presence of distinguishable landmarks which are needed for the five-point registration method. Currently, the landmarks are marked during the preoperative CT-scan by attaching radiopaque lead stickers to anatomical features such as the nipple, birthmarks, or scars. If the number of recognizable features is not sufficient, additional landmarks are drawn on manually with a marker. The first in-house experiences with this workflow have shown that the selection of landmarks is prone to user-dependent errors and inaccuracies easily stack up due to the manual steps that are required. Thus, there is a need for a more robust registration method that requires fewer manual steps and is not dependent on explicit anatomical features.

Secondly, the conventional AR system is only suitable for tumour localisation prior to incision. However, the surgeons from our centre have reported that they also see potential to use the HoloLens post-incision, as a reference and guidance for resection once the skin has been opened. If the conventional AR system is to be used post-incision, the reference QR code should be sterile and remain in the surgical field for the whole procedure. Subsequently, in-house testing showed that the ability of the HoloLens to accurately track the QR code and update the position of the hologram is often lacking. This insufficient tracking causes a misalignment of the holographic overlay and often requires a new registration procedure to update the hologram's position. However, as the anatomical landmarks on the skin are inaccessible once the first incision has been made, it is impossible to perform a new registration with the use of the current AR system. Hence, a second need is to explore the feasibility of other registration methods that allow registration post-incision, i.e. on the exposed surface of the ribs. With such a system, the HoloLens could be used to locate the affected rib and tumour easily and accurately prior to incision, and subsequently guide the resection once the skin and chest have been opened. This would reduce the complexity of intraoperative tumour localisation and circumvent the need for multiple imaging techniques that are conventionally used during surgery.

A registration method that could possibly fulfil these needs is surface matching. Surface matching registration methods find the most optimal transformation between two large sets of points, i.e. point clouds, that make up a surface[28,29]. For example, a transformation between the surface point cloud of the skin in the OR and the corresponding surface point cloud derived from preoperative images. Surface matching does not require the preoperative selection of anatomical landmarks, and therefore would circumvent the user-dependent errors that arise with the conventional landmark-based registration method.[30] Additionally, surface matching makes it possible to perform registration on only a sub patch of the total reference surface. This means that registration can be performed even if the anatomical structure is not fully exposed during surgery.[31] It is therefore hypothesized that surface matching could also be a suitable method to perform registration on the exposed surface of the ribs and allow registration post-incision.

An important step during surface matching is the acquisition of a point cloud of the surface in the OR. This intraoperative surface point cloud can be obtained by different acquisition methods, each having their own benefits and limitations. Common methods are the use of a

tracked pointer, a laser scanner or depth camera.[32–34] These examples mostly find their applications in neurosurgery or maxillofacial surgery, as surface matching especially shows good results on explicit surface features like the nose or edges of the jaw. Less literature exists on the use of surface matching methods on anatomical structures with no explicit surface features, for example the thorax or ribs. It is therefore still unknown whether surface matching is a feasible method for registration during chest wall resections. Furthermore, it should still be explored which surface acquisition method would be most suitable for this application.

This thesis explores the feasibility of surface matching for the use of AR during paediatric chest wall resections. Therefore, two different surface acquisition methods were developed and evaluated. The first method uses a tracked pointer which is traced across the surface of the thorax or ribs, to capture the intraoperative point cloud. The second method captures this point cloud with the Time-Of-Flight (ToF) camera of the HoloLens 2. Both surface matching methods were compared to the conventional landmark-based registration method to investigate which registration technique has the best potential to be used during paediatric chest wall resections, both pre-incision and post-incision. Consequently, the outcomes of this thesis can contribute to the further optimalisation of the conventional AR system for intraoperative tumour localisation, hereby improving surgical management of paediatric chest wall Ewing sarcoma.

1. Clinical background

Ewing sarcoma

Ewing sarcoma (ES) is the second most common bone tumour in children and constitutes 10% to 15% of all bone sarcomas[4]. It was first described by James Ewing in 1921 as a radiosensitive round-cell sarcoma thought to originate from the blood vessels in the bone tissue[35,36]. Current research mainly suggests an origin in mesenchymal or neural crest-derived stem cells, though the exact origin of ES is still a subject of debate.[7,37,38]

ES may occur in any bone or soft tissue, but is mostly found in the tubular bones of the extremities (45%), thorax or abdomen (20%), or the pelvis (20%)[4,7]. The incidence of ES is higher in Caucasians than in Asians and Africans, with a slight predilection for males.[2,5,39] It is mostly diagnosed in children and young adolescents, with a mean age of 15[1,5,39,40]. In the Netherlands, around 13 children are diagnosed with ES every year[3,40].

ES is a high-risk tumour and approximately 25% of the patients present with metastases at the time of diagnosis, usually found in the lungs (70-80%) or bones (40-45%)[4,6–8]. Metastatic disease is an independent risk factor for a poor prognostic outcome with a 5-year overall survival (OS) of solely 30%[8,41]. Other risk factors include large tumour volume, older age, male sex and an axial tumour location[42]. Patients with localized disease have a significantly better 5-year OS of 75% or higher, mainly because of the advances in therapeutic management that have been accomplished over the years.[8,41–43]

Diagnosis

The most common symptoms of ES include localized pain or a palpable mass at the tumour site. Other symptoms are unexplained fatigue, weight loss or fever.[44,45] With symptoms being variable and nonspecific, early diagnosis of ES remains challenging.

Diagnosis is based on a combination of imaging techniques such as ultrasonography, radiography, magnetic resonance imaging (MRI), computed tomography (CT) and position emission tomography (PET) to examine the extend of the tumour and the presence of metastases.[6] On radiography or CT images, ES can be recognized by an aggressive pattern of permeative osteolysis, lamellated periosteal reaction (so called “onion skin”), or mineralization of the bone matrix.[6,46] MR imaging often shows a soft-tissue mass together with marrow replacement and cortical destruction[47]. The signal intensity on T1 and T2 can be heterogeneous, though ES usually presents as a low intensity mass on T1 and a high intensity on T2[6]. The tumour shows a prominent gadolinium uptake in contrast enhanced T1 images.[6,46,47]

Diagnostic imaging is always combined with a biopsy to allow histological assessment of the tumour tissue. This assessment shows sheets of monotonous small round blue cells with prominent nuclei, minimal cytoplasm and positive CD99 immunostaining. The presence of a t(11:22) translocation differentiates ES from other paediatric small round cell tumours.[48] Histological assessment is mainly used to find a definitive diagnosis and less for prognosis of the disease, as studies have not yet reached consensus on prognostic markers within ES.[7,48]

Subsequently, all diagnostic techniques are combined to confirm the diagnosis of ES and to determine the most effective therapeutic strategy.[6,45]

Treatment

In the Netherlands, all paediatric patients are treated according to the Interim Ewing Protocol. Regardless of the extend of disease, all patients start with nine intensive cycles of chemotherapy. Patients receive a combination of vincristine, doxorubicin, and cyclophosphamide (VDC) followed by ifosfamide and etoposide (IE) after an interval of 14 days. Eventually, patients receive five cycles of VDC intermitted with four cycles of IE. After the third and sixth cycle, imaging is repeated to evaluate tumour response and to determine the appropriate strategy for local treatment through radiotherapy and/or surgery. If possible, resection of the tumour is always the first option

for local control. However, it can be combined with preoperative radiotherapy for patients that show clinical progression under chemotherapy or when the tumour is (yet) inoperable. During surgery, the main goal is to achieve wide tumour resection margins. Secondly, another major aim is conservation of the limb or limitation of the defect created by resection. Consequently, the resection margins should be wide enough for optimal oncological control but narrow enough to maximize function. In case of insufficient margins, surgery is often combined with postoperative radiotherapy to assure local control.

After local treatment, patients receive postoperative chemotherapy according to their risk group defined in the Interim Ewing Protocol. Patients with localized disease and good tumour response are considered 'good risk' and will receive another three cycles of IE intermitted with two VC cycles. Patients with localized disease but a poor tumour response, or patients with large tumour volumes are stratified as 'poor risk'. These patients receive one cycle of both IE and VC, followed by a high dose chemotherapy (HDT) treatment with busulfan-melphalan (BuMel). Patients with metastasized disease receive five more cycles of intermitted VDC-IE, often combined with radiotherapy. Additionally, treosulfan-melphalan HDT (TreoMel-HDT) followed by autologous stem-cell reinfusion may be considered for high risk patients.[11,49–51]

Chest-wall resections

For ES of the ribs, local treatment consists of a chest wall resection. As literature has shown that a complete resection with wide margins leads to the best long-term outcome, it is most common to remove the affected rib together with parts of the adjacent ribs.[16,43,52,53] This makes a chest wall resection an invasive procedure that might lead to significant thorax deformities especially in young children that are not full grown. As deformities of the thorax can lead to impairments in breathing and mobility, chest wall resections require an extensive surgical planning to determine the most optimal outcome. Hence, a patient specific planning is made based on a preoperative CT scan and the previous MR images. This plan should allow safe and wide resection planes, while saving as much healthy tissue as possible.

During surgery, the majority of patients is placed in lateral decubitus position with the affected side up. Dual lumen intubation is used to deflate the ipsilateral lung to create space in the pleural cavity if necessary. Additionally, patients will receive an epidural catheter, arterial line and venous access lines, available for urgent fluid administration when needed.[15]

After the patient has been correctly prepared and positioned, the first step during surgery is an accurate tumour localisation. This is of utmost importance to execute the surgical planning and to achieve safe tumour margins. However, ES of the ribs are often invisible or nonpalpable due to the tumour growing in medial direction and their response to preoperative chemotherapy. Consequently, several techniques are used to locate the affected rib and to map the extend of the tumour prior to resection. Surgeons generally use a combination of palpation, thoracoscopy, fluoroscopy, ultrasonography and radiography to locate the tumour as accurately as possible, though no generalized approach exists.[15,17]

Once the correct resection planes and corresponding incisions are established, the affected ribs are exposed and resected. The Interim Ewing protocol prescribes a resection with wide tumour margins according to Enneking, meaning that the resection planes are histologically negative.[11,54] In practice, ES are commonly resected with a 1-4 cm margin around the tumour.[15,16,55]

Depending on the size of the resulting defect, reconstruction is needed to restore chest wall rigidity, protection for underlying organs, preserve respiratory function and to achieve good cosmetic results.[56] The most commonly used reconstruction materials are the non-rigid Gore-Tex® and Marlex® mesh.[57] These materials are biologically inert and minimize the potential for lung adhesions. The mesh is tensioned inside the defect to create an airtight seal. Subsequently, a thorax drain is positioned, and the skin is closed in layers. Most patients are then transferred to the Intensive Care for postoperative recovery and monitoring.[15]

Long-term outcomes

Given the intensity of ES therapy, patients are at high risk of developing long-term complications after treatment has ended.[58] A study by Hamilton et al. (2017) showed that at least 77% of the long-term survivors of ES (≥ 5 years) suffers from long-term complications.[8] Half of the patients experience complications with musculoskeletal abnormalities due to surgery or radiotherapy, such as amputation, bone deformities, or limb length discrepancies. For patients that underwent a chest wall resection due to ES of the ribs, the most common musculoskeletal complication is scoliosis. The removal of affected ribs decreases the attractive force on the ipsilateral side of the thorax and therefore increases the load on the contralateral side, which can lead to significant deformities of the vertebral column. Studies show that 25-43% of patients develop scoliosis after a chest wall resection, the severity depending on the age, location of the tumour and size of the surgical defect.[12,52,59,60] Of these patients, 39% requires corrective spinal surgery.[53]

Another common long-term complication in paediatric oncology is cardiovascular toxicity, which is mainly caused by anthracyclines in chemotherapy agents or radiation on the chest.[61] Around 28% of ES survivors develop some form of cardiac dysfunction, such as pericardial disease or cardiomyopathy.[8,62] Other prevalent complications after the treatment of ES are infertility, endocrine dysfunction or psychiatric illness.[8]

The presence of these long-term effects can have a significant impact on the Quality of Life (QoL) of ES survivors. A recent study by Kadan-Lottick et al. (2022) showed that ES survivors are at an increased risk for reporting neurocognitive difficulties, such as difficulties with task efficiency or emotional regulation.[63] Furthermore, survivors tend to have lower QoL scores when comparing their physical abilities to healthy control subjects.[64] Fortunately, when comparing mental health and overall QoL scores, the difference between ES survivors and healthy subjects remains minimal.[64,65] This indicates that survivors generally manage to adapt to their physical limitations by changing their internal standards, i.e. the response shift, which consequently results in normal QoL scores.[66,67]

Clinical challenges

This thesis focusses on the clinical challenges that arise during the surgical management of chest wall Ewing sarcoma. As mentioned before, the intraoperative localisation of these tumours is a complex process. Since chest wall Ewing sarcomas are generally invisible and nonpalpable from the outside, finding the affected rib only by visual inspection and palpation is extremely difficult. Therefore, surgeons generally use multiple imaging techniques to locate the rib and tumour as accurately as possible prior to incision. Not only is this a time-consuming process; intraoperative tumour localisation remains a challenge when the tumour has become invisible due to neo-adjuvant chemotherapy, even with invasive imaging techniques like thoracoscopy. Consequently, there have been case reports of chest wall resections where incorrect ribs were removed. As chest wall resections can lead to significant deformities that negatively affect respiration, mobility and aesthetics, removal of incorrect ribs must be prevented at all times. This emphasizes the need to improve and facilitate the intraoperative tumour localisation during paediatric chest wall resections.

This thesis aims to reduce the complexity of intraoperative tumour localisation by exploring the use of surgical guidance through Augmented Reality (AR). With AR, a virtual model of the affected ribs and tumour can be directly projected onto the patient in the OR. AR could thus serve as a quick, non-invasive, and intuitive visualisation technique and therefore significantly facilitate surgical planning and management of chest wall resections. The next chapter gives an introduction to AR and describes the basic principles of using AR for guidance during surgery.

2. Technical background

Augmented Reality

Augmented Reality is a visualisation technique to project virtual objects or environments into the real world. With AR, an interactive and immersive environment can be created to enhance the user's experience, or to add in the user's enjoyment or understanding. Over the last couple of years, AR has gained popularity in many fields and applications, such as gaming, education, tourism, marketing and manufacturing.[68] AR is commonly applied through smartphones or tablets, with examples like Snapchat photo filters, the Pokémon Go game, or the visualisation of virtual furniture into your own interior (Figure 1).

Another way of applying AR is through a Head Mounted Display (HMD). In this case the user wears a device with semi-transparent displays, on which the virtual content is projected while the vision of the real environment is preserved. Popular HMD's are the Google Glass, Magic Leap and Microsoft HoloLens 2.[69,70] The ability to project models directly in the user's field of view brings numerous advantages. It provides the user with better ergonomics, hand-eye coordination, perception of the virtual content and a more intuitive experience than AR through a phone or tablet.[69] Additionally, an HMD is a hands-free device, and thus allows the user to still use their hands for certain tasks or to interact with the virtual model.

Based on these advantages, HMD's have also shown great potential in the field of healthcare. Currently, HMD's are already being used as a therapeutic tool in the treatment of patients, to train or educate medical professionals, or as an additional tool during surgical procedures.[71] For example, HMD's can be used preoperatively to examine the patient's anatomy in 3D and to determine a patient-specific surgical plan. Intraoperatively, an HMD can be used to visualise the planned resection, or guide the placements of trocars or incisions. Though the use of AR through HMD's is currently being explored in almost any medical field, the most popular applications lie within the field of neurosurgery, maxillofacial surgery, orthopedics and laparoscopic surgery.[23]

Figure 1. *Examples of Augmented Reality.* ***Left****: AR through a smartphone, to visualise virtual furniture.* ***Right****: AR through an HMD (the HoloLens 2), for surgical guidance.*

Registration

When using an HMD as a guidance during surgery, the alignment of the virtual model with the patient in the OR should be as accurately as possible. This alignment is achieved by performing a registration procedure. Registration describes the process of geometrically aligning two or more images or scenes taken at a different times or angles[72]. For example, the alignment of a virtual 3D model to the real location of the patient in the OR. The virtual model is generally derived from preoperative images and is therefore defined in a different coordinate frame than the patient in the OR. During the registration procedure, alignment of the model is achieved by finding the most

optimal transformation matrix between the different coordinate frames.[73] The next section of this chapter describes the mathematical concept of such a registration procedure.

Consider we have two coordinate frames A and B, which are scaled, translated, and rotated versions of each other. A point $\mathbf{p}$ is represented in B by ${}^{B}\mathbf{p}$. The same point is presented in A by:

$$ {}^{A}\mathbf{p} = s\,{}^{A}\mathbf{R}_{B}\,{}^{B}\mathbf{p} + {}^{A}\mathbf{t}_{B} \quad (1) $$

Here s is a scaling factor, and ${}^{A}\mathbf{t}_{B}$ is a 3D vector that describes the translation between the two coordinate frames, i.e. the translation of frame B with respect to frame A:

$$ {}^{A}\mathbf{t}_{B} = \begin{bmatrix} {}^{A}t_{x} \\ {}^{A}t_{y} \\ {}^{A}t_{z} \end{bmatrix} \quad (2) $$

The rotation between the two frames is described by the 3x3 rotation matrix ${}^{A}\mathbf{R}_{B}$:

$$ {}^{A}\mathbf{R}_{B} = \begin{bmatrix} \cos(\varphi_{xx}) & \cos(\varphi_{xy}) & \cos(\varphi_{xz}) \\ \cos(\varphi_{yx}) & \cos(\varphi_{yy}) & \cos(\varphi_{yz}) \\ \cos(\varphi_{zx}) & \cos(\varphi_{zy}) & \cos(\varphi_{zz}) \end{bmatrix} \quad (3) $$

Where φ_{xx} is the angle between the x-axis in A ($\mathbf{x}_A$) and the x-axis in B ($\mathbf{x}_B$), φ_{xy} is the angle between $\mathbf{x}_A$ and $\mathbf{y}_B$, and so on. The scaling factor, translation vector, and rotation matrix can be combined into one 4x4 homogenous transformation matrix ${}^{A}\mathbf{T}_{B}$:

$$ {}^{A}\mathbf{T}_{B} = \begin{bmatrix} s\,{}^{A}\mathbf{R}_{B} & & & {}^{A}\mathbf{t}_{B} \\ 0 & 0 & 0 & 1 \end{bmatrix} \quad (4) $$

With ${}^{A}\mathbf{T}_{B}$ we can describe the direct transformation, including translation, rotation, and scaling, of a point $\mathbf{p}$ in frame B to frame A:

$$ {}^{A}\underline{\mathbf{p}} = {}^{A}\mathbf{T}_{B}\,{}^{B}\underline{\mathbf{p}} \quad (5) $$

The use of homogeneous transformation matrices makes it easier to calculate transformations between more than two coordinate frames. When using an HMD during surgery, we are generally dealing with multiple coordinate frames. For example, separate coordinate frames are defined for the HoloLens (the HMD), the patient, and the preoperative 3D model. By combining all transformation matrices for each coordinate frame to another, we can compute the correct transformation of the preoperative model into the HoloLens coordinate frame:

$$ {}^{HL}\underline{\mathbf{p}} = {}^{HL}\mathbf{T}_{patient}\,{}^{patient}\mathbf{T}_{model}\,{}^{model}\underline{\mathbf{p}} \quad (6) $$

In order to solve this equation, a patient registration should be performed. During the registration procedure, the correct transformation matrix from the preoperative model to the patient in the OR can be computed by different methods and algorithms.[74] Within this thesis, two different registration methods are considered: landmark-based registration and surface matching. Both methods will be further explained in the next section of this chapter.

Landmark-based registration

Landmark-based registration describes the process of aligning two small sets of points. Within surgical context, these points are defined as a set of anatomical landmarks, which are features that can be easily recognized on the patient in the OR and in the preoperative images.[74] Examples of anatomical landmarks are features such as the nose or eyes, corners of bones, or bifurcations of important vessels.[75,76] Anatomical landmarks can also be created manually, for example by

attaching artificial markers to the patient during the preoperative scan. These can be non-invasive markers such as radiopaque lead stickers, as well as more invasive bone screws.[27,77]

During the registration procedure, the positions of the anatomical landmarks in the OR can be obtained through different tracking methods, for example by using external electromagnetic (EM) or optical tracking systems.[78,79] With the use of an HMD, e.g. the HoloLens, the intraoperative position of the anatomical landmarks can also be derived by internal tracking through the HoloLens camera, for example by using a surgical pointer with a QR code.[27,34] After obtaining the intraoperative positions of the anatomical landmarks, they can be directly correlated to the virtual position of the landmarks in the preoperative images by computing the transformation matrix between the two sets of points.

Procrustes algorithm

To compute the transformation matrix between the patient and the preoperative images, a commonly used method is the Procrustes algorithm. This algorithm consist of several steps to align two sets of points as accurately as possible.[73] Consider we have a set of five landmarks that are selected on the patient with use of a pointer tracked by the HoloLens; ${}^{HL}\mathbf{p}_n$ with n = 1,…,5 (Figure 2a). These points correspond to the set of landmarks in the preoperative CT scan; ${}^{CT}\mathbf{p}_n$ (Figure 2b):

$$ {}^{HL}\mathbf{p}_n = s\,{}^{HL}\mathbf{R}_{CT}\,{}^{CT}\mathbf{p}_n + {}^{HL}\mathbf{t}_{CT} \qquad (7) $$

The first step in the Procrustes algorithm is to calculate the centroids, i.e. the means, of the set of points within each frame. By subtracting the mean from each set of points, the translation between the two frames is ruled out (Figure 2c). Secondly, the scale (s) is calculated by taking the ratio between the deviations of each set of points. Subsequently, the points in the reference frame (the CT points) are neutralized for this scale (Figure 2d). After the points are compensated for the scaling, the rotation matrix between both frames (${}^{HL}\mathbf{R}_{CT}$) can be calculated. This is done by the Kabsch algorithm, which is a method to calculate the most optimal rotation matrix between two frames by use of singular value decomposition (SVD).[80] The final step is the calculation of the translation vector (${}^{HL}\mathbf{t}_{CT}$), which follows directly from Equation 7. Consequently, the CT points can be transformed into the HoloLens coordinate frame and be projected onto the patient in the OR (Figure 2e).[73]

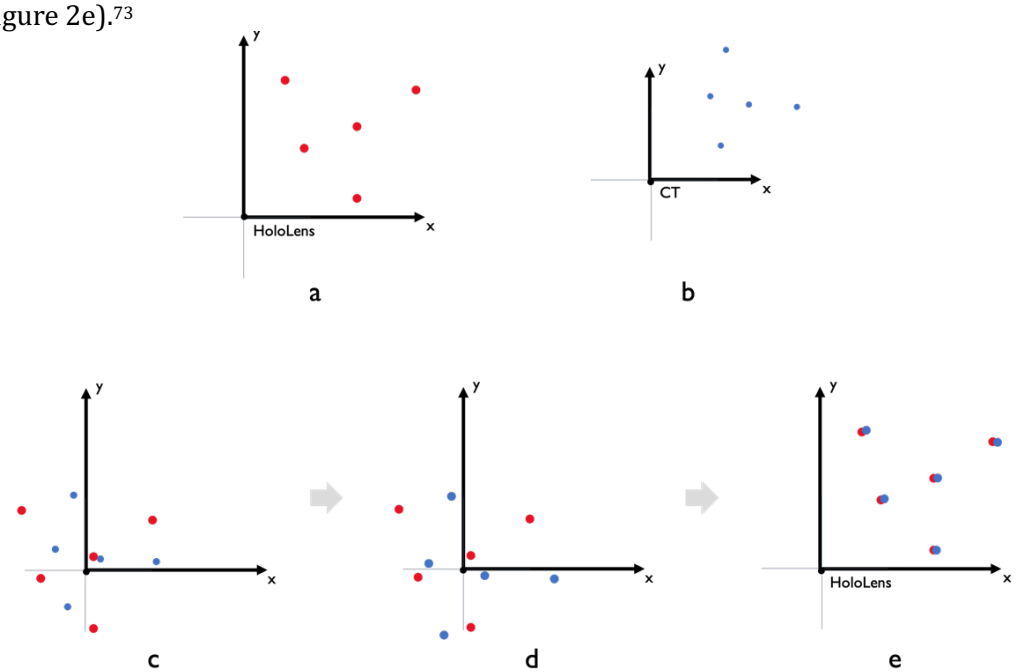

Figure 2. *Procrustes algorithm illustrated.* ***a)*** *Five landmarks selected with a pointer tracked by the HoloLens.* ***b)*** *The corresponding five landmarks in the preoperative CT scan. Note that the landmarks are translated, rotated, and scaled versions of each other.* ***c)*** *The two sets are neutralized for translation by subtraction of the centroids.* ***d)*** *The set of CT points is neutralized for the scale.* ***e)*** *The most optimal rotation matrix is obtained through SVD, and the CT points are transformed into the HoloLens coordinate frame.*[73]

Surface matching

Another commonly used registration method is surface matching.[31] Surface matching is a registration method that is used to align two corresponding surfaces. In order to perform computations on these surfaces, they should be considered as a mesh, which is a digital 3D object composed of vertices and faces. Vertices represent the surface as a large collection of points defined in a 3D Cartesian coordinate system, a so-called point cloud (Figure 3a). This point cloud is divided into smaller sets of three connected vertices which make up the faces, also called triangles or polygons, of the mesh (Figure 3b).

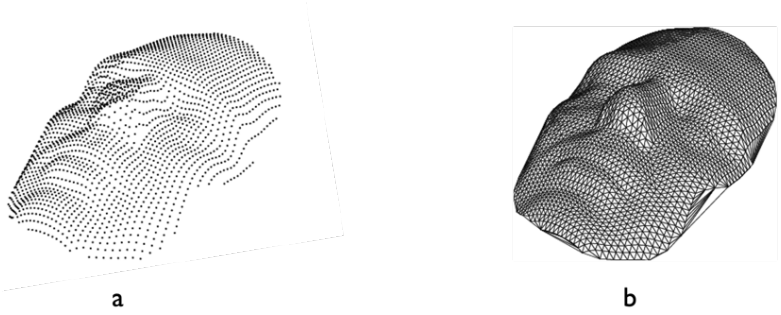

***Figure 3**. Surface of the face visualised as a mesh. **a)** The vertices, or point cloud, of the surface. **b)** The faces of the surface.[81]*

Within medical applications, surface matching can be performed on surfaces of anatomical structures, for example the surface of the skin, an organ or bone.[32,82,83] A preoperative point cloud of the surface can be derived by the segmentation of these structures from preoperative images and saving them as a mesh object. Subsequently, the obtained surface point cloud can be used for registration.

During registration, the preoperative point cloud is matched to the corresponding intraoperative surface of the concerning structure. For example, a preoperative point cloud of the patient's head is matched to the patient's head in the OR (Figure 4). To realize this, the intraoperative surface of the patient's head should also be defined as a point cloud. This can be achieved through different surface acquisition methods. Common methods are the use of a tracked pointer, a laser scanner or an (RGB) depth sensor (Figure 4b).[32–34] Subsequently, the most optimal transformation matrix between the two corresponding point clouds can be computed, and the preoperative surface can be registered to the intraoperative situation (Figure 4c).

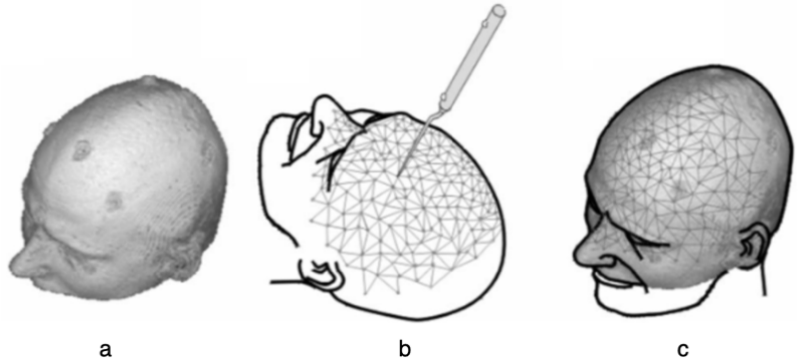

***Figure 4**. Example of surface matching on the head. **a)** Surface of the skin, reconstructed from preoperative imaging. **b)** Acquisition of the corresponding point cloud in the OR with a tracked pointer. **c)** Alignment of the two surfaces after registration.[84]*

An advantage of surface matching is that it is no longer required to locate specific anatomical landmarks prior to surgery. This reduces the complexity of the preoperative workflow and the risk of user dependent errors. Additionally, most surface matching algorithms do not require the corresponding point clouds to have the same number of points. Consequently, registration can be performed on only a sub patch of the total surface. This makes it possible to perform registration even if the organ or anatomical structure is not fully exposed during surgery.[31]

Iterative Closest Point algorithm

The most common algorithm to compute the transformation matrix between two corresponding point clouds is the Iterative Closest Point (ICP) algorithm. The ICP algorithm considers one point cloud as a fixed reference and transforms the other point cloud to best match this reference point cloud. For example, in Figure 4 the intraoperative surface of the patient's head is kept as the reference, and the preoperative point cloud is transformed to align with the patient's head in the OR. The most optimal transformation is iteratively estimated by minimizing the squared distances between the corresponding points of the two point clouds. This process consists of multiple steps:[85]

Consider a reference point cloud $\mathbf{p}_i$ and a corresponding preoperative point cloud $\mathbf{q}_i$, which is a rotated and translated version of $\mathbf{p}_i$ (Figure 5a). The first step in the ICP algorithm is to match each point in $\mathbf{q}_i$ with its nearest point in $\mathbf{p}_i$. These matched points form the correspondence pairs (Figure 5b). The next step is to estimate the transformation (consisting of a rotation matrix $\mathbf{R}$ and a translation vector $\mathbf{t}$) which will best align each correspondence pair. Mathematically, this transformation is estimated by minimizing the squared distance between the transformed point cloud $\mathbf{q}_i$ and the reference point cloud $\mathbf{p}_i$ (Figure 5c):[86,87]

$$\min_{\mathbf{R},\mathbf{t}} \sum_i \|\mathbf{p}_i - (\mathbf{R}\mathbf{q}_i + \mathbf{t})\|^2 \qquad (8)$$

The estimated transformation is then applied to the point cloud $\mathbf{q}_i$ and all steps of the algorithm are repeated. New correspondence pairs are formed and again the most optimal transformation is estimated and applied to $\mathbf{q}_i$. This means that with each iteration, the two point clouds become closer and more aligned with each other. Eventually, the solution reaches convergence, meaning that alignment won't improve any further and the most optimal transformation is found. In practice, this iterative process can lead to long computation times. Consequently, thresholds are often used to limit the number of iterations or to stop convergence at a certain level.[87]

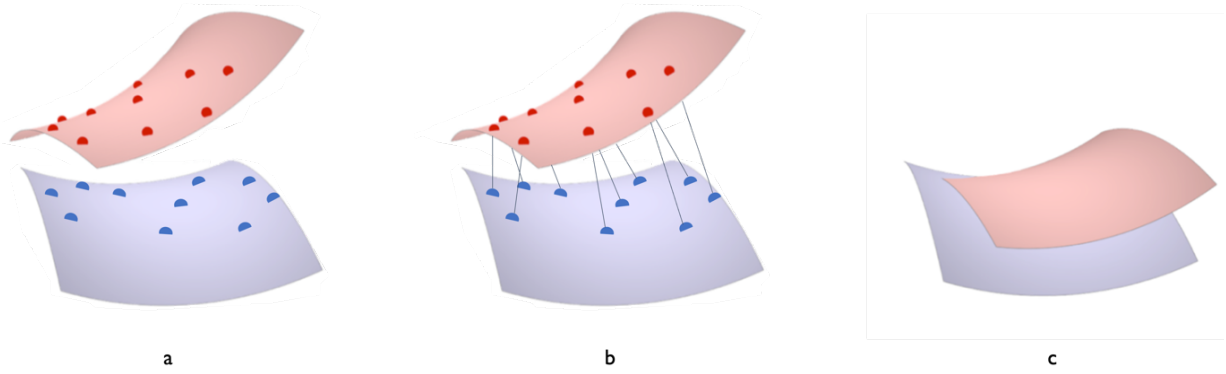

Figure 5. *ICP algorithm illustrated.* ***a)*** *Selected points in a point cloud of a surface (red).* ***b)*** *Find the closest points in the corresponding point cloud (blue).* ***c)*** *The transformation is calculated by minimizing the distances between the points. All steps are iterated until convergence is reached.*[88]

A disadvantage of the ICP algorithm is that it does not guarantee that the computed transformation matrix is the overall best solution. As the correspondence pairs are solely based on the closest distance between points, it is possible that the algorithm gets 'trapped' into a solution that brings the point clouds very close, but not aligned perfectly with each other. This is called a local minimum. It means that locally, the algorithm has returned the best solution, but an even better solution (a so-called global minimum) exists. Consequently, to prevent the algorithm from getting trapped in local minima, ICP algorithms generally require some form of an initial transformation step to globally align the two point clouds before starting the actual ICP registration process.[32]

Augmented Reality for paediatric chest wall resections

A recent in-house study by Spijkerboer et al. (2022) has explored the feasibility of AR in paediatric chest wall resections[27]. The HoloLens 2 was used to visualise a virtual model of the ribs and tumour prior to incision. To align the virtual 3D model with the real position of the patient in the OR, Spijkerboer et al. used a five-point registration method based on anatomical landmarks, such as the nipple, birthmarks, or scars. However, the first in-house experiences with this workflow have shown that the selection of landmarks is prone to user-dependent errors and inaccuracies easily stack up due to the manual steps that are required. Thus, there is a need for a more robust registration method that requires fewer manual steps and is not dependent on explicit anatomical features.

Secondly, the landmark-based registration method is only suitable for tumour localisation prior to incision. However, the surgeons from our centre have reported that they also see potential to use the HoloLens post-incision, as a reference and guidance for resection once the skin has been opened. To realize this, a new registration should be performed after the ribs are exposed. However, as the anatomical landmarks on the skin are inaccessible once the first incision has been made, it is impossible to perform a new registration with the use of the conventional AR system.

Surface matching could be a solution to these challenges, as it does not require the localisation of anatomical landmarks. Additionally, it is thought that surface matching could be used to perform registration directly on the post-incision surface of the exposed ribs. However, literature on the use of surface matching methods on anatomical structures with no explicit surface features, for example the thorax or ribs, is scarce. It is therefore still unknown whether surface matching is a feasible method for registration during chest wall resections. Furthermore, it should still be explored which surface acquisition method would be the most suitable for this application. This thesis explores the feasibility of surface matching for the use of AR both pre- and post-incision during paediatric chest wall resections. Therefore, two common surface acquisition methods were developed and evaluated based on their accuracy and applicability.

The first method acquires a surface point cloud of the patient in the OR by tracing a pointer across the patient's skin or exposed chest wall. The pointer contains a QR code through which the position of the tip can be tracked by the HoloLens 2. The registration procedure is similar to the method described by Liebmann et al. (2019)[34], who used a 3D printed pointer to capture the surface of vertebrae during spinal surgery. An advantage of acquiring the surface point cloud with a surgical pointer is that it doesn't require the anatomical structure to be fully exposed, as it allows the user to capture the exposed surface very selectively.[89,90] For the use of chest wall resections, it is therefore hypothesized that this acquisition method would especially be suitable for the registration post-incision.

The second acquisition method captures the intraoperative surface point cloud by use of the Time-of-Flight (ToF) depth camera inside the HoloLens 2. With this ToF camera, a depth image of a surface is automatically obtained by measuring the phase delay of reflected infrared (IR) rays. Literature on the use of a depth camera for registration has proven it to be quick, automatic and less prone to user dependent errors than landmark-based methods.[30,91,92] However, a disadvantage of automatic depth cameras it that they generally capture a large and non-selective surface. This means that the acquired point cloud easily contains noise that might reduce the accuracy of registration.[92,93] Within the application of chest wall resections, surface acquisition with a ToF camera is therefore thought to be most suitable for registration pre-incision.

3. Objectives

The main goal of this thesis is to improve the conventional AR system for the surgical localisation of paediatric chest wall Ewing sarcoma. The new system should reduce the complexity of the preoperative workflow and the user-dependent errors that currently arise with landmark-based registration. Furthermore, the new system should allow registration post-incision, to let surgeons use the HoloLens as an extra guidance once the skin has been opened.

This thesis investigates the applicability of surface matching as a new registration method that could be applied both pre-incision and post-incision during paediatric chest wall resections. However, no literature exists on the use of surface matching on the thorax or the ribs. Thus, a first step is to explore the feasibility of surface matching on a surface without explicit features, such as the thorax. The second step is to explore whether surface matching can be used to perform registration directly on the ribs to allow the use of AR post-incision. Within this thesis, the feasibility of surface matching is investigated by comparing two different surface acquisition methods. The first method uses a surgical pointer which is traced along the contour of the patient's skin or exposed ribs to acquire a point cloud that can be used for registration. The second method acquires this point cloud with the Time-Of-Flight camera of the HoloLens 2.

To reach the main goal of this thesis, several research questions are considered:

1. What is the feasibility of surface matching as a registration method for tumour localisation prior to incision?
2. What is the accuracy of both surface matching methods compared to landmark-based registration?
3. Does surface matching result in better performances based on registration times, user-friendliness and registration complexity compared to landmark-based registration?
4. To what extend can we use surface matching as a registration method post-incision?
    - Which surface acquisition method can perform a registration on the exposed surface of the ribs the most accurately?
    - What is the potential of registration post-incision based on the surgeon's experience?

Thesis outline

This thesis explores the feasibility of surface matching by comparing two different surface acquisition methods. The software design and technical background of both surface matching methods are described in Chapter 4.

To validate their performances and to compare their results with the conventional landmark-based registration method, a phantom study was performed (Chapter 5). All three registration methods were compared based on their accuracy, registration time, and inter-observer variability. Chapter 6 describes the results of a human cadaver study that was performed to investigate the performance of surface matching in clinical practice. To test the feasibility of the two surface matching methods, two surgeons performed a chest wall resection with the use of the newly developed AR systems. Both surface matching methods were compared based on their ability for registration prior to incision, as well as registration directly on the ribs. Subsequently, surgeons completed a questionnaire to evaluate on the system's potential, user-friendliness and added value of AR during surgery.

The results of the two studies are combined in Chapter 7, which gives a general discussion and complete overview of the feasibility of surface matching and AR during paediatric chest wall resections.

4. Software design

Confidential.

5. Phantom study

Comparison of different registration methods for the use of Augmented Reality during chest wall resections

Introduction

In the last couple of years, Augmented Reality has gained popularity in many surgical fields. AR allows the direct visualisation of anatomical structures onto the patient in the OR, and can therefore facilitate surgical guidance and decision making.[18–21] AR has already proven to be of added value in maxillofacial surgery, neurosurgery, and orthopaedics.[21–26] A recent study by Spijkerboer et al. (2022) has explored the feasibility of AR for the intraoperative localisation of paediatric chest wall tumours.[27] These tumours have often become invisible and non-palpable due to preliminary chemotherapy, making intraoperative localisation of the affected rib a complex and time-consuming process that requires multiple imaging modalities, depending on the tumour's extend, depth and position[15]. Surgeons generally use a combination of the preoperative CT and MR images, as well as intraoperative imaging techniques such as echography, thoracoscopy or fluoroscopy to localize affected rib and tumour and plan the resection. The used techniques differ per patient and thus no generalized approach for tumour localisation yet exists.[15,17]

The use of AR during paediatric chest wall resections has the potential to facilitate surgical tumour localisation by projecting a virtual model of the affected ribs, tumour, and anatomical structures directly onto the patient in the OR. The conventional AR system of Spijkerboer et al. uses a landmark-based registration method to project the virtual model prior to incision with the HoloLens 2. The first experiences with this system are promising and surgeons see the potential of using the HoloLens 2 for intraoperative tumour localisation during chest wall resections. However, since the intraoperative tumour localisation is conventionally based on multiple imaging techniques and no golden standard exists, surgeons find it difficult to quantify the accuracy of the holographic overlay in the OR. Hence, before surgeons can fully rely on the localisation based on the AR system, the projection accuracy should be validated.

Furthermore, in-house experiences with the conventional landmark-based registration method have shown that the current AR system is prone to user dependent errors and inaccuracies easily occur. Thus, there is a need to explore other registration methods to improve the conventional AR system. This thesis therefore explores the feasibility of surface matching, which allows a more automatic registration without the need for additional manual steps or the preoperative localisation of anatomical features. Additionally, the algorithms that are generally used for surface matching make it possible to perform registration on only a sub patch of the total surface. This means that registration can be performed even if the organ or anatomical structure is not fully exposed during surgery.[31] It is therefore expected that within paediatric chest wall resections, surface matching could be used for registration post-incision, e.g. directly on the surface of the ribs. This would make it possible to provide surgeons with holographic guidance once the skin has been opened.

This phantom study explores the feasibility of surface matching for the use of the HoloLens 2 during paediatric chest wall resections. Therefore, two different surface acquisition methods are considered. Both methods are compared to the conventional landmark-based registration method based on their accuracy, registration times and inter-observer variability.

Materials & Methods

The feasibility of surface matching was investigated by comparing the two different surface acquisition methods that are described in Chapter 4 of this thesis: contour registration and ToF camera registration. Both methods were tested on a pre-incision and post-incision surface of a 3D printed phantom of a paediatric thorax, i.e. on the surface of the skin, and the exposed chest wall respectively.

Phantom design

The phantom was designed by use of a preoperative CT-scan of a paediatric patient who underwent a chest wall resection of the sixth to eighth rib. During this preoperative CT scan, the patient was positioned in lateral decubitus position and radiopaque lead stickers were attached to scars and birthmarks to serve as anatomical landmarks. A 3D model of the patient was created by manual segmentation of the thorax in 3D Slicer (Version 5.0.3, The Slicer Community, http://www.slicer.org[108]) (Figure 14a). Additionally, to simulate registration on the post-incision surface, the exposed surface of the ribs and chest wall was manually reconstructed to mimic the operating field after the skin has been opened (Figure 14b).

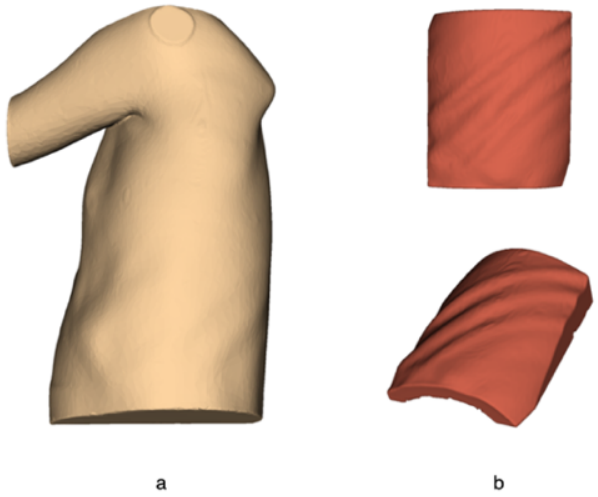

Figure 6. *3D models created in 3D Slicer.* ***a)*** *Segmentation of the thorax, used for registration pre-incision.* ***b)*** *Reconstructed surface of the operating field (exposed rib 6,7 and 8) for registration post-incision.*

Subsequently, the 3D models were transferred to Fusion 360 (Version 2.0.15995, Autodesk, Inc., San Francisco, CA, USA) and redesigned into a phantom that could be used for multiple registration purposes. Therefore, two different panels were designed. The first panel included pivots at the exact locations of the anatomical landmarks in order to validate the landmark-based registration method (Figure 15a). The second panel was used for both surface matching methods, and consisted of a smooth skin surface in which five beacon points were included for accuracy measurements (Figure 15b). Registration post-incision could be tested by removing the skin panel and hereby exposing the surface of the ribs and chest wall (Figure 15c). Like the skin panel, five beacon points were included in this surface to allow accuracy measurements based on registration post-incision.

The phantom was 3D printed true to size in white polylactic acid (PLA) with the Ultimaker S5. As the material and lighting conditions of the phantom can have an effect on the performance of a ToF camera, the phantom was painted in realistic colours to minimize the effect of these possible errors.[103]

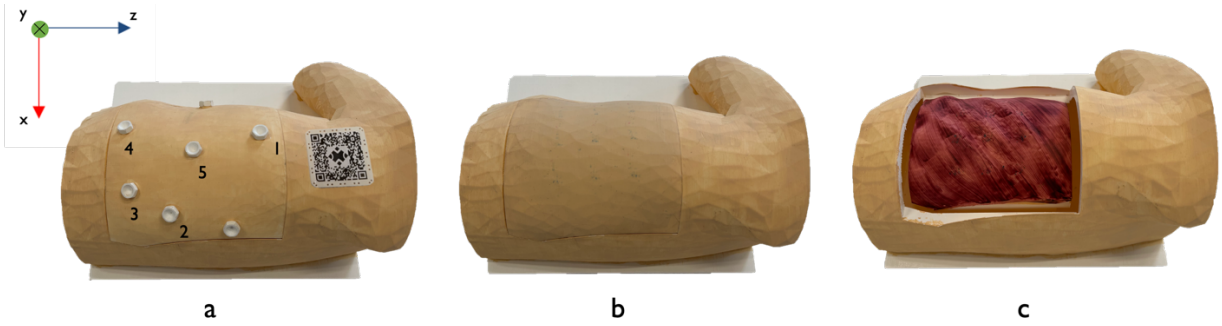

Figure 7. *3D printed phantom with different registration surfaces.* ***a)*** *Panel used for landmark-based registration. The five indicated pivots were used for registration.* ***b)*** *Panel used for both surface matching methods.* ***c)*** *Post-incision registration surface.*

Registration

The technical background and software design of all three registration methods is described in Chapter 4 of this thesis. Like the workflow for actual chest wall resections, the HoloLens application was prepared by implementing the surface meshes of the skin and exposed chest wall of the phantom into Unity. In order to enable accuracy measurements, the Unity applications were adjusted to project nine target points instead of an anatomical 3D model (Figure 16).

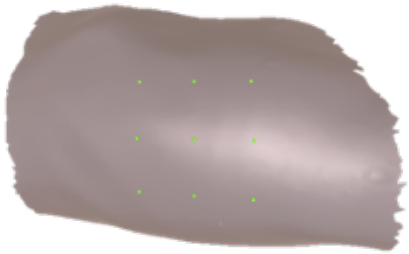

Figure 8. *The nine target points that were projected onto the phantom after each registration.*

During all phantom experiments, the registrations were performed with the user standing at the dorsal side of the phantom, as this corresponds to the surgeon's position during surgery. The user was instructed to maintain this position while performing the accuracy measurements to minimize the effect of drift. All experiments were performed in a room without natural lighting, to eliminate ToF camera differences caused by varying lighting conditions between experiments, and to simulate the lighting conditions in the OR. Subsequently, the next factors were considered for each registration method specifically:

Method 1: Landmark-based registration

Landmark-based registration was performed with the five anatomical landmarks indicated in Figure 15a and the reference QR code attached to the cranial side of the phantom. During registration, the Vuforia system shows the tracked position of the pointer's tip by projecting a green overlay onto the 3D printed pointer. However, inaccuracies inside the Vuforia system can cause a mismatch between the physical position of the pointer and the green overlay. Within these phantom experiments, the holographic overlay of the pointer was therefore always seen as truth.

When registration was succeeded, the panel with pivots was changed for the panel with beacon points to perform the accuracy measurements.

Method 2: Contour registration

Contour registration was performed by tracing the surgical pointer across the whole surface of the skin panel or exposed chest wall surface (Figure 17), as this gave the most accurate results during preliminary testing. During registration, the user was instructed to keep the head as still as possible to reduce the risk of drift while acquiring the point cloud of the surface.

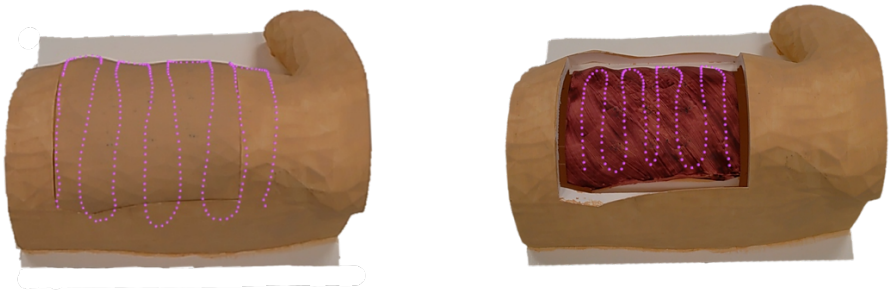

Figure 9. *Example of the acquired point cloud (pink spheres) during contour registration.* ***a)*** *Registration pre-incision.* ***b)*** *Registration post-incision.*

Method 3: ToF camera registration

During ToF camera registration, the depth maps were acquired from a dorsal, diagonal perspective according to the surgeon's position during surgery. The user was instructed to keep its head approximately 30-50 cm from the phantom, as preliminary tests showed that this position resulted in the most accurate depth maps.

Accuracy measurements

The registration accuracy of the three methods was validated by means of two experiments. The experiments were performed by two observers, both an experienced and unexperienced HoloLens user. In the first experiment, the accuracy of all three registration methods was validated prior to incision. Per observer, each registration method was timed and repeated five times. After each registration was completed, nine target points were projected onto the phantom. The user was instructed to objectively mark the positions of each target with a pencil, while keeping their head as still as possible to eliminate the effect of drift. Subsequently, a digital calliper with 0,01 mm accuracy was used to measure the 2D distance between the marked points and the five beacon points in the panel of the phantom. Using these measurements, the 3D position of the marked points was computed in Python with the use of the trilateration principle (Appendix C).[109] Subsequently, the Target Registration Error (TRE) was calculated for each target. The TRE was defined as the Root Mean Square error (RMS), or Euclidian distance, between the 3D positions of the marked targets and the 3D positions of the virtual targets. Additionally, the separate errors in x-, y-, and z-direction were calculated to examine systematic shifts into a certain direction.

The second experimented investigated the feasibility of the two surface matching methods for registration post-incision. The landmark-based registration was not included in this experiment as it is impossible to perform registration post-incision with use of landmarks on the skin.

During the second experiment, the same validation experiment was performed by the two observers. Registration was performed on the surface of the exposed ribs and chest wall, and each registration method was timed and repeated five times. Like the first experiment, nine target points were projected onto the phantom and again the TRE's and systematics shifts were calculated with the use of five beacon points and trilateration principle.

Statistical analysis

For the first experiment, a one-way ANOVA test was performed to investigate whether there was a significant difference between the TRE's of the three registration methods. Subsequently, a post-hoc Tukey's test was performed to compare the registration methods in pairs to discover which methods were significantly different from each other. For the second experiment, a student T-test was performed to compare the TRE values of both surface matching methods. Additional student T-tests were used to analyse the inter-observer variability in TRE values and registration times for each registration method during both experiments.

Results

Per registration method and observer, nine target measurements were performed five times, resulting in a total of 90 TRE measurements per registration method for both experiments. Table 1 shows the results of the accuracy measurements for the first experiment. The average standard deviations were calculated based on the standard deviation of each registration moment (e.g. five per method and observer).

The ToF camera registration was proven to be the fasted registration method with an average time of 26 ± 11 seconds. The landmark-based registration and contour registration were performed in 35 ± 10 and 84 ± 42 seconds respectively. The statistical analysis showed no significant difference in registration times between the landmark-based registration and ToF camera registration ($p = 0{,}723$). The contour registration method was significantly slower than the other two registration methods ($p < 0{,}001$).

The biggest inter-observer variability in registration times was seen in the contour registration method, with an average registration time of 52 ± 2 seconds for the experienced observer (Observer 1) compared to 115 ± 38 seconds for the unexperienced observer (Observer 2) ($p < 0{,}05$). For the other two registration methods, the differences in registration times between the observers were less evident, though the statistical analysis showed a significant difference for the landmark-based registration method ($p < 0{,}05$).

Landmark-based registration resulted in the most accurate projections, with an average TRE of 2,3 ± 2,3 mm, which was significantly lower than both surface matching methods ($p < 0{,}001$). The contour registration method and ToF camera registration method had an average TRE of 6,5 ± 1,9 mm and 7,7 ± 2,1 mm respectively and were not significantly different ($p = 0{,}162$).

The errors in x-, y- and z-direction do not show evident systematic shifts for any of the registration methods, as all values are close to zero and the standard deviations are small. The biggest shift is seen in the results of the ToF camera registration for Observer 2. The error in the x-direction of -7,3 ± 1,4 mm showed that the targets were mostly shifted towards the ventral side of the phantom.

Table 1. *Results of the accuracy measurements for the registration pre-incision.*

Method	Subgroup	Time ± std (s)	TRE ± std (mm)	Error x ± std (mm)	Error y ± std (mm)	Error z ± std (mm)
Landmark-based registration	Observer 1	27 ± 3	2,4 ± 1,0	0,7 ± 1,0	-0,74 ± 1,0	0,1 + 0,9
	Observer 2	43 ± 8	2,2 ± 1,2	0,1 ± 0,9	-0,6 ± 1,2	-0,4 ± 1,2
	Mean	**35 ± 10**	**2,3 ± 2,3**	**0,4 ± 0,9**	**-0,7 ± 1,1**	**-0,2 ± 1,0**
Contour registration	Observer 1	52 ± 2	2,9 ± 0,8	1,4 ± 0,5	-0,9 ± 1,0	0,7 ± 0,8
	Observer 2	115 ± 38	10,1 ± 0,8	0,4 ± 0,9	0,1 ± 3,8	1,2 ± 0,8
	Mean	**84 ± 42**	**6,5 ± 1,9**	**0,9 ± 0,7**	**-0,4 ± 2,8**	**0,9 ± 0,8**
ToF camera registration	Observer 1	21 ± 3	5,0 ± 0,9	2,5 ± 0,7	-1,2 ± 1,8	2,5 ± 1,1
	Observer 2	32 ± 13	10,3 ± 1,1	-7,3 ± 1,4	1,3 ± 3,9	-0,9 ± 1,4
	Mean	**26 ± 11**	**7,7 ± 2,1**	**-2,4 ± 1,1**	**0,0 ± 3,0**	**0,8 ± 1,3**

The inter-observer variability in TRE values for each registration method is visualised in Figure 18. The violin plot shows the distribution of the total collection of TRE measurements for all targets (e.g. 90 measurements per registration method and observer). The student T-tests showed no significant difference between the TRE of Observer 1 and 2 for the landmark-based registration method ($p = 0{,}613$). However, the violin plot and statistical analysis show an evident difference between the TRE values for both surface matching methods ($p < 0{,}001$).

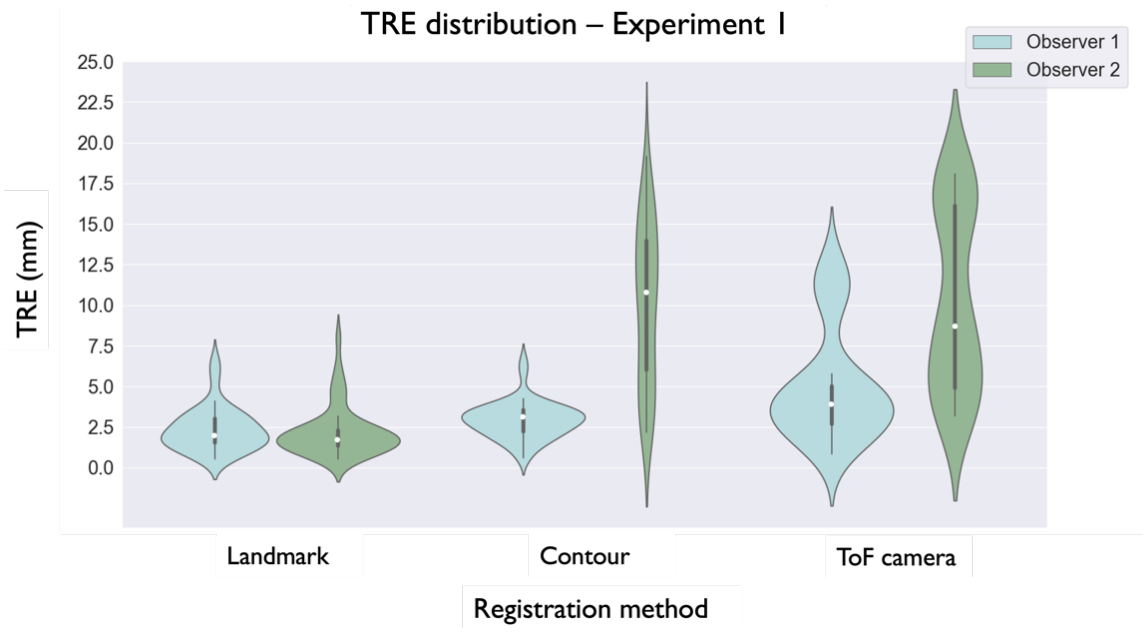

Figure 10. *Violin plot of the TRE values for each observer and registration method during the first experiment. The median TRE values are represented by the white dot.*

Table 2 shows the results of the accuracy measurements for the post-incision experiment. Again, the ToF camera registration was the fastest method with a mean time of 20 ± 8 seconds, compared to 51 ± 6 seconds for the contour registration method ($p < 0{,}001$). There was no significant difference between the registration times for each observer.

The ToF camera registration showed the highest accuracy with a mean TRE of 4,3 ± 1,8 mm, compared to 6,2 ± 5,0 mm for the contour registration method ($p < 0{,}001$). When looking at the errors in x-, y-, and z-direction, again no distinct shifts towards a specific direction can be concluded. The biggest shift is seen towards the positive x-axis for both registration methods, meaning that the targets were slightly shifted to the dorsal side of the phantom.

Table 2. *Results of the accuracy measurements for the registration post-incision.*

Method	Subgroup	Time ± std (s)	TRE ± std (mm)	Error x ± std (mm)	Error y ± std (mm)	Error z ± std (mm)
Contour registration	Observer 1	51 ± 5	4,9 ± 2,2	1,6 ± 2,7	-0,1 ± 1,8	-1,7 ± 2,7
	Observer 2	51 ± 7	7,4 ± 1,4	5,8 ± 1,4	1,1 ± 2,0	-2,9 ± 1,3
	Mean	**51 ± 6**	**6,2 ± 5,0**	**3,7 ± 2,1**	**0,5 ± 1,9**	**-2,3 ± 2,1**
ToF camera registration	Observer 1	18 ± 4	3,9 ± 0,7	2,3 ± 0,6	-0,3 ± 1,5	0,3 ± 0,9
	Observer 2	22 ± 10	4,7 ± 1,0	4,1 ± 1,0	-0,2 ± 1,4	1,0 ± 0,7
	Mean	**20 ± 8**	**4,3 ± 1,8**	**3,2 ± 0,8**	**-0,3 ± 1,4**	**0,6 ± 0,8**

The inter-observer variability in TRE values for the second experiment is visualised in Figure 19. Like in the first experiment, the student T-tests showed a significant difference between Observer 1 and 2 for the contour registration method ($p < 0{,}001$). No significant difference between was found within the results of the ToF camera registration ($p = 0{,}074$).

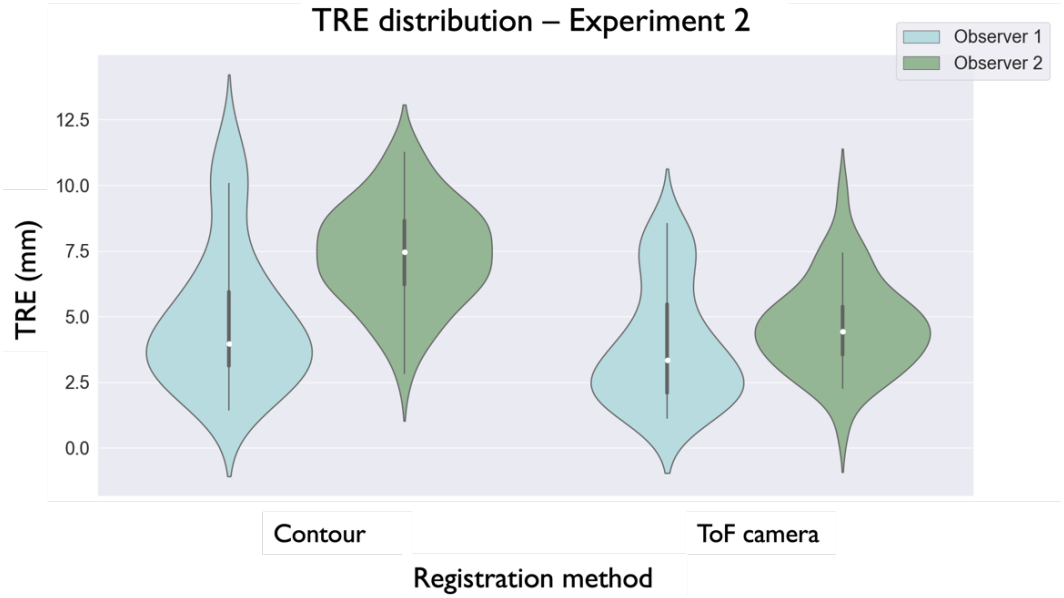

Figure 11. *Violin plot of the TRE values for each observer and registration method during the second experiment. The median TRE values are represented by the white dot.*

Discussion

This phantom study compared three registration methods based on their accuracy, registration times and inter-observer variability, during a pre-incision and post-incision experiment. For registration pre-incision, the conventional landmark-based registration method showed the lowest TRE and inter-observer variability. The ToF camera registration method was the fasted registration method with an average time of solely 26 seconds. The largest inter-observer variability was seen with the contour registration method, for both accuracy and registration times.

For registration post-incision, the ToF camera registration showed the best results with faster registration times and a significantly lower TRE than the contour registration method. Again, the contour registration method showed the most inter-observer variability, with a significant difference in TRE values between the two observers.

Based on the results of this phantom study, the two surface matching methods were not more accurate than conventional landmark-based registration. However, the clinical challenges that usually arise with the landmark-based registration method, e.g. the user-dependent errors, or inaccuracies in the landmark configuration, could not be taken into account within the design of this phantom study. As the landmark-based registration was performed on a rigid panel with pivots at the exact locations of the landmarks, the registration could be performed very accurately, and inter-observer variability was easily eliminated. Meanwhile, both surface matching methods were still prone to inter-observer variabilities, as their registration workflow required multiple user-dependent steps. For example, the manual selection of the total surface in contour registration, or the observer's line-of-sight while acquiring the depth map with the ToF camera. Though the results of the landmark-based registration give a good impression of how accurate the registration can be when performed in an ideal situation, they cannot be directly compared to the results of both surface matching methods within this phantom study.

When evaluating the results of the surface matching methods alone, this phantom study proves that surface matching on the surface of the thorax or exposed chest wall is feasible. The accuracy results of both surface matching methods show that it is possible to localise targets with a TRE below 1 cm. Within our clinical application, i.e. the localisation of the affect rib, this accuracy would be sufficient.

There are several aspects which could explain the higher TRE values of the surface matching methods for both accuracy and registration times compared to the landmark-based

registration method. Firstly, the higher TRE of the contour registration method is probably caused by the inexperience of Observer 2. When comparing the contour registration method with the other two methods, the registration workflow of the contour method is the least straightforward and requires the most manual steps. For unexperienced users, this method is therefore more prone to inaccuracies in the acquired point cloud compared to the other registration methods. When looking at the accuracy results of first experiment for the experienced user, the contour registration method had an average TRE of 2,9 ± 0,8 mm, which is comparable to the TRE of the landmark-based registration method. Furthermore, the inter-observer variability is less evident in the second experiment, where Observer 2 already gained more skill with using the HoloLens. It is thus hypothesized that when the user gains more experience and agility with this contour registration method, the results will significantly improve and inter-observer variability will decrease.

The higher TRE values for the ToF camera registration method could possibly be explained by the fact that there was an offset within the ToF camera. Preliminary phantom testing showed that the acquired depth map had a systematic error of approximately 1-2 cm in the direction of sight. Consequently, when performing registration based on this depth map, the hologram is systematically positioned too far away from the user and the position of the targets is strongly dependent on the user's perspective. Within this phantom study, the effect of this offset was minimized by instructing the user to keep their head as still as possible during registration and demarcation of the targets. However, this does not guarantee that registration and demarcation were performed from the exact same perspective, and thus shifts could have easily occurred.

The effect of the depth offset can be seen when comparing the errors in the x-direction of both observers. For Observer 2, the hologram had a systematic shift in the x-direction of -7,3 ± 1,4 mm during the first experiment, meaning that the targets were shifted towards the ventral side of the phantom. This confirms the expected offset into the direction of sight. However, this shift is not seen in the same results for Observer 1, or within the results of both observers during the second experiment. The observers might have been standing closer to the phantom when marking the targets, causing the line of sight to be more from above and the shift to be less evident.

Though the results of both experiments give a good impression of the applicability of surface matching on a surface like the thorax or ribs, there are a few limitations that should be considered when interpreting these results for clinical implementation. First, the experiments were performed on a rigid, 3D printed phantom, meaning that the surface meshes from the CT images matched the acquired point clouds on the phantom exactly. This is not in accordance with the real situation, where there will always be a slight difference in the position of the patient during the preoperative CT scan and the position in the OR. A different position causes changes in the curvature of the thorax, and therefore creates a mismatch between the configuration of the anatomical landmarks, or the surfaces to be registered. Consequently, it is expected that registration accuracies will be lower when using these registration methods during actual chest wall resections.

Another limitation of this phantom study is that the post-incision surface resembled a very simplified version of the actual surgical field once the skin has been opened. The surface used in this phantom study contains clear curvatures of the ribs, but it is difficult to predict whether the actual post-incision surface will contain the same exposure. Furthermore, the post-incision surface of the phantom was quite large and fully accessible, while in reality, the size of the incision and the presence of surrounding tissues will limit the accessibility of the exposed surface. The results of the post-incision experiment therefore only indicate that it is possible to reach a sufficient registration accuracy based on the curvature of the ribs. However, the actual post-incision registration performance of the surface matching methods cannot be concluded based on this phantom study.

The limitations of this phantom study can be resolved by testing the registration methods in a more realistic setting. For example, the tests could be performed on a non-rigid phantom with more realistic features, or on human cadavers. For registration pre-incision, it could be investigated whether surface matching still results in sufficient registration results when there

are slight thorax deformations between the preoperative CT and the intraoperative situation. Furthermore, by performing these experiments on cadavers, it can be investigated whether post-incision registration can still be performed on a less exposed surface that corresponds to the actual surgical field during chest wall resections. Consequently, although the results of this phantom study prove the feasibility of surface matching on the thorax and exposed ribs, testing in realistic setting will make the necessary translation into clinical practice.

Conclusion

This phantom study showed that it was feasible to perform surface matching on the pre-incision surface of the thorax and post-incision surface of the ribs with sufficient accuracies and registration times. Conventional landmark-based registration was still proven to be more accurate for registration pre-incision. However, the accuracy measurements based on a rigid 3D printed phantom cannot be directly correlated to the clinical situation, where user-dependent errors and thorax deformations can affect the registration accuracy. Consequently, the registration methods should still be validated in a more realistic setting before a statement can be made about their implementation during chest wall resections.

6. Cadaver study

Applicability of surface matching for Augmented Reality guidance during paediatric chest wall resections

Introduction

The phantom study in the previous chapter shows that it is feasible to perform surface matching on the pre-incision surface of the skin and post-incision surface of the ribs with sufficient accuracy. However, the experiments were performed on a rigid, 3D printed phantom, meaning that the preoperative surfaces matched the acquired point cloud on the phantom exactly. This is not in accordance with the clinical setting, where there will always be a slight difference between the position of the patient during the preoperative CT scan and the position in the OR. This difference in position could change the curvature of the thorax, and therefore influence the accuracy of registration. Consequently, to translate the results of the phantom study to clinical practice, the surface matching methods should first be tested in a more realistic setting.

Furthermore, the surface that was used for registration post-incision was a very simplified version of the actual surgical field once the skin has been exposed. The phantom study showed that it was possible to achieve accurate registrations on this surface with both surface matching methods. However, based on these results it cannot be concluded that the surface matching methods will give the same accuracies in the surgical situation, as the actual post-incision surface might not be fully accessible for registration and the presence of surrounding tissues and instruments might negatively influence registration performances.

Consequently, to make the necessary translation of phantom tests into clinical practice, the next step is to validate both surface matching methods in a setting that mimics the surgical situation as realistically as possible. This chapter therefore describes the cadaver study that was performed to explore the applicability of the surface matching methods during actual chest wall resections. Within this clinical application, the registration method would be considered applicable if surgeons are able to locate the correct ribs based on the projections of the HoloLens. During this cadaver study, the main research question therefore was: "Are the registration accuracies of the two surface matching methods sufficient to locate the correct rib during surgery?" To answer this question, two experiments were performed in which the feasibility of both methods for registration pre- and post-incision was investigated.

Materials & Methods

In this study, two paediatric oncologic surgeons performed cadaver experiments to test the applicability of the newly developed surface matching methods for the surgical localisation of chest wall tumours. During these experiments, the surgeons each operated on a separate fresh-frozen cadaver of a human thorax. The study consisted out of two individual experiments. During the first experiment, the two surface matching methods were compared to the conventional landmark-based registration method by means of their registration accuracy pre-incision. During the second experiment, the surgeons performed a simulated chest wall resection on the cadavers with the use of AR guidance through the HoloLens 2. Within this experiment, both surface matching methods were used to perform registration pre-incision and post-incision. Subsequently, a postoperative CT scan was made to analyse the accuracy of the resection. After each experiment, surgeons were asked to evaluate the performance and added value of the registration methods by means of a questionnaire. (Appendix D).

Preoperative workflow

The preoperative workflow and software settings for all three registration methods were the same as described in Chapter 4 of this thesis. To prepare the virtual model and HoloLens applications, a preoperative CT scan was made. Radiopaque lead stickers were attached to manually created landmarks in order to allow landmark-based registration. The landmarks were selected on the rigid parts of the thorax, e.g. on the sternum and area below the breasts, to circumvent possible configuration differences caused by tissue deformations between the preoperative CT scan and intraoperative situation.

Virtual models of the skin, post-incision surface, sternum, ribs and an imaginary tumour were created in 3D Slicer (Version 5.0.3, The Slicer Community, http://www.slicer.org[108]) by manual segmentation (Figure 20a). Subsequently, the surface areas used for surface matching were manually selected in Meshmixer (Autodesk, Inc., San Francisco, CA, USA). Like the placement of the landmarks, the pre-incision surface of the skin was selected on the rigid parts of the thorax below the breasts (Figure 20b). The post-incision surface was estimated by selecting a wide margin around the affected and adjacent ribs to cover the whole surgical area as good as possible (Figure 20c).

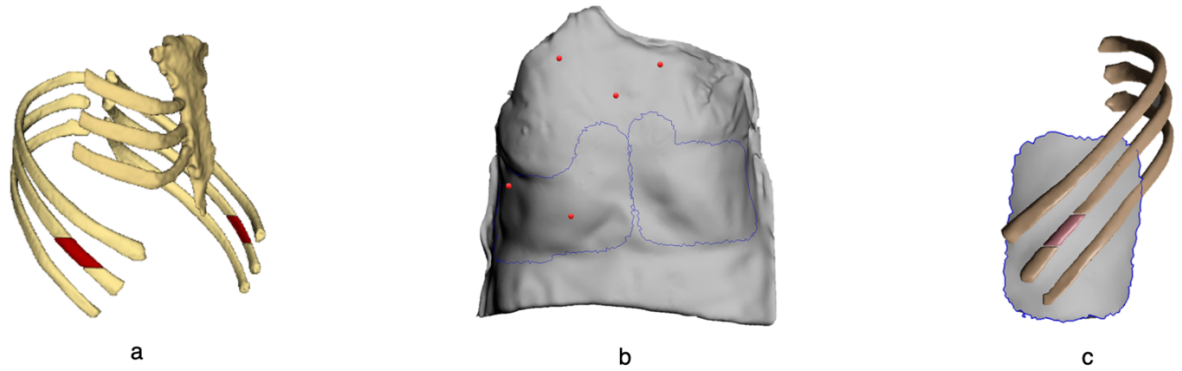

***Figure 12**. Examples of the virtual 3D model, landmarks and surfaces used for registration. **a)** Virtual model of the sternum, rib seven, eight and nine, and imaginary tumour (red). **b)** Five landmarks (red spheres) and selected surfaces on the skin (delineated in blue) for registration pre-incision. **c)** Selected surface of exposed ribs (grey area, delineated in blue) used for registration post-incision.*

Experiment 1

In the first experiment, the registration accuracy of the two surface matching methods was compared with the conventional landmark-based registration method based on the registration performance prior to incision. The surgeons performed each registration method once based on the landmarks and the pre-incision surface of the skin. Each registration was performed on the same side of the cadaver, e.g. in the example shown in Figure 20, both surface matching methods were performed on the selected surface on the right side of the thorax. After registration was achieved, a hologram of the sternum with six target points on ribs three, four and five, was projected onto the cadaver (Figure 21a). After each registration, the surgeon was instructed to objectively demarcate the six target points on the skin with a coloured marker (Figure 21b). Subsequently, radiopaque lead stickers were attached to all demarcated points to compare the results of each registration method by use of a postoperative CT scan. Finally, the surgeons completed a questionnaire to evaluate on the ease and applicability of each registration method.

All demarcated points were segmented from the postoperative CT scan in 3D Slicer and reconstructed into the sets of six points corresponding to each registration method. To transform the points from the postoperative CT scan into the virtual model of the sternum, a registration procedure was performed. First, the sternum and affected ribs were segmented from the postoperative CT scan to create a postoperative model that was the same as the preoperative model as visualised in Figure 20a. The postoperative model was then registered to the preoperative model with the use of the open-source software CloudCompare (Version 2.12.3, Open GL, R&D EDF) which contains an ICP registration function. Within CloudCompare, the preoperative model was selected as the reference surface mesh and subsequently the ICP algorithm returned the optimal transformation matrix which aligned the two virtual models. This

transformation matrix was then applied to the segmented demarcated points to transform them into the preoperative model of the sternum. Consequently, the demarcated points could be directly compared to the target points in the projected hologram.

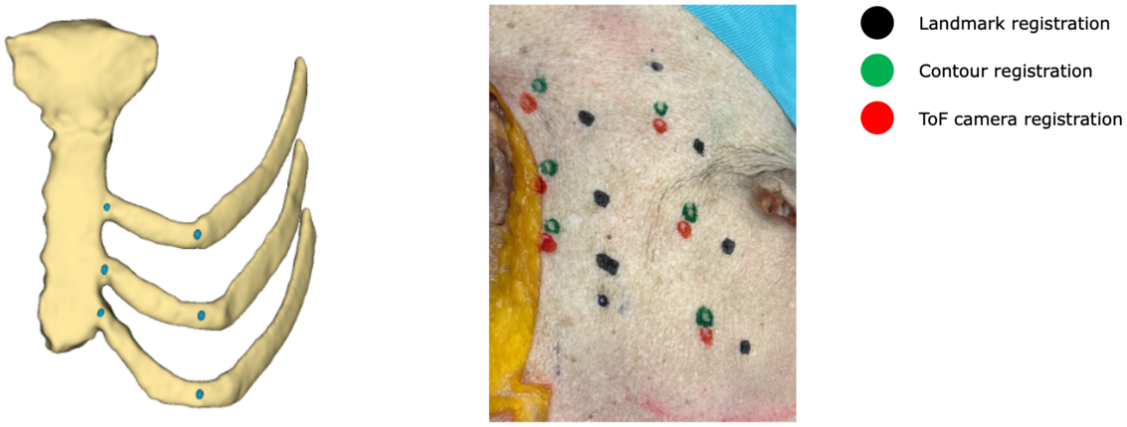

***Figure 13**. Examples of hologram and demarcated points for Experiment 1. **a)** Virtual model of the sternum and target points (blue) that was projected onto the cadaver after each registration. **b)** Demarcated target points after landmark-based (black), contour (green), and ToF camera registration (red).*

Experiment 2

In the second experiment, the feasibility of using the surface matching methods for surgical guidance during chest wall resections was evaluated. The two surgeons performed a simulated chest wall resection with use of the HoloLens 2 both pre-incision and post-incision. A resection of the imaginary tumour in the eighth rib was simulated on both sides of the thorax, each side using a different surface matching method. Figure 22 shows an example of the experiment using the contour registration method on the right side of the thorax.

The experiment was designed to simulate the real surgical situation. Therefore, the surgeons were allowed to assess the virtual 3D model of the cadaver, consisting of the affected ribs and imaginary tumour, before starting the resection (Figure 20a). The surgeons were then asked to locate the affected rib based on palpation alone and mark this location with a coloured marker.

Subsequently, the HoloLens was used to project the virtual model onto the cadaver (Figure 22a). Depending on the cadaver and resection side, this was done by either contour registration or ToF camera registration on the selected surface of the skin (Figure 20b). Again, the surgeon was asked to mark the location of the tumour with a marker (Figure 22b). Like in the real surgical situation, the surgeons had to plan the resection according to their own interpretation of the anatomy and accuracy of the holographic projection. Before making the first incisions and starting the actual resection, the surgeons filled in a questionnaire to evaluate on the localisations based on palpation and the HoloLens alone, and to indicate whether the use of the HoloLens changed their surgical decision making and confidence in localisation of the tumour.

Subsequently, the surgeons continued the resection by exposing the ribs and chest wall. Once exposed, the same registration method was performed on the post-incision surface of the ribs and the virtual model was projected onto the surgical field (Figure 22c). The surgeons were then asked to mark the edges of the tumour with a surgical saw based on their own interpretation of the anatomy, preoperative assessment of the virtual model, palpation and the holographic projection (Figure 22d). Ultimately, the surgeons completed the same questionnaire to evaluate the registration performance on the post-incision surface. The same experiment was then repeated on the other side of the cadaver with use of the second surface matching method. After both experiments were completed, the surgeons completed another questionnaire about the general potential and added value of using the HoloLens for intraoperative tumour localisation during chest wall resections.

Finally, a postoperative CT scan was made to compare the marked tumour edges with the virtual model to assess the accuracy of resection on both sides. The affected ribs and marked tumour were therefore segmented from the postoperative CT scan and the same transformation matrix that was derived in the first experiment was used to register the postoperative model with the preoperative model. Consequently, the performed resection could be directly compared to the imaginary tumour to assess whether the surgeons were able to locate the correct rib and perform an accurate resection with use of the surface matching methods.

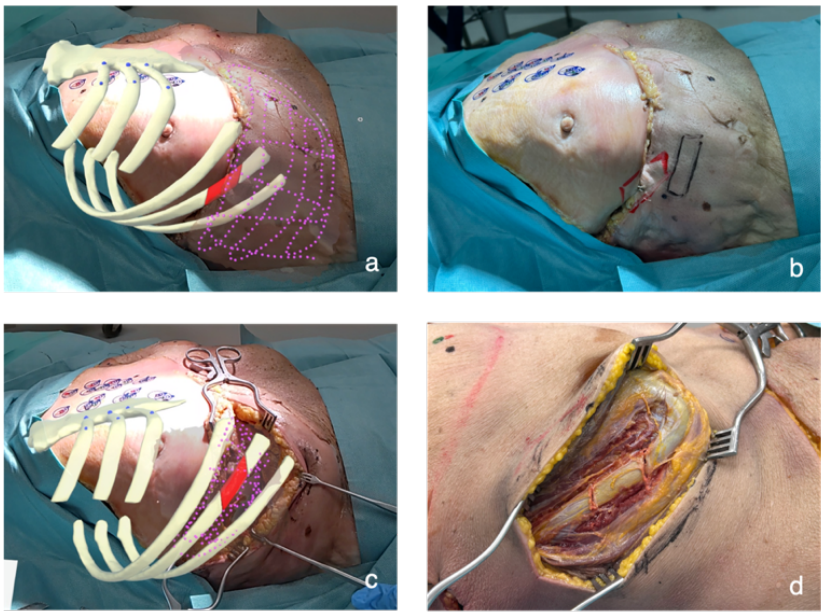

Figure 14. *Example of the simulated chest wall resection performed on the right side of the cadaver using the contour registration method.* ***a)*** *The contour registration method is used to perform registration pre-incision, resulting in a projection of the affected ribs and tumour onto the cadaver.* ***b)*** *Delineation of the tumour based on palpation (black) and holographic overlay (red).* ***c)*** *Result of the registration on the surface of the exposed ribs and chest wall.* ***d)*** *Tumour edges demarcated with a surgical saw.*

Results

Experiment 1

The results of the first experiment are visualised in Figure 23. For Surgeon 1 (Figure 23a) the landmark-based registration was the most accurate, though the projected target points were slightly shifted towards the lateral side. For Surgeon 2 (Figure 23b) the landmark-based registration method also showed the most accurate results, as the demarcated points are almost perfectly aligned with the virtual target points. It is remarkable that the difference between the accuracy of the two surgeons is quite significant, as the positions of the anatomical landmarks were similar for both cadavers. The results of this experiment therefore confirm the user-dependency of the landmark-based registration method.

When looking at the results of both surface matching methods, Surgeon 1 saw an evident misalignment of the sternum after registration. However, the contour registration method still projected the target points onto the correct ribs. For the ToF camera registration, the target points were shifted in the cranial direction, which resulted in the demarcation of incorrect ribs.

Surgeon 2 indicated that the projections of both surface matching methods seemed accurate. The visualisation in Figure 23b show that the projections of both methods were shifted towards the medial direction, though the target points were still projected onto the correct ribs. The size of the shift is approximately the same for both methods, which indicates that there might have been a deformation of the skin between the preoperative CT-scan and intraoperative situation.

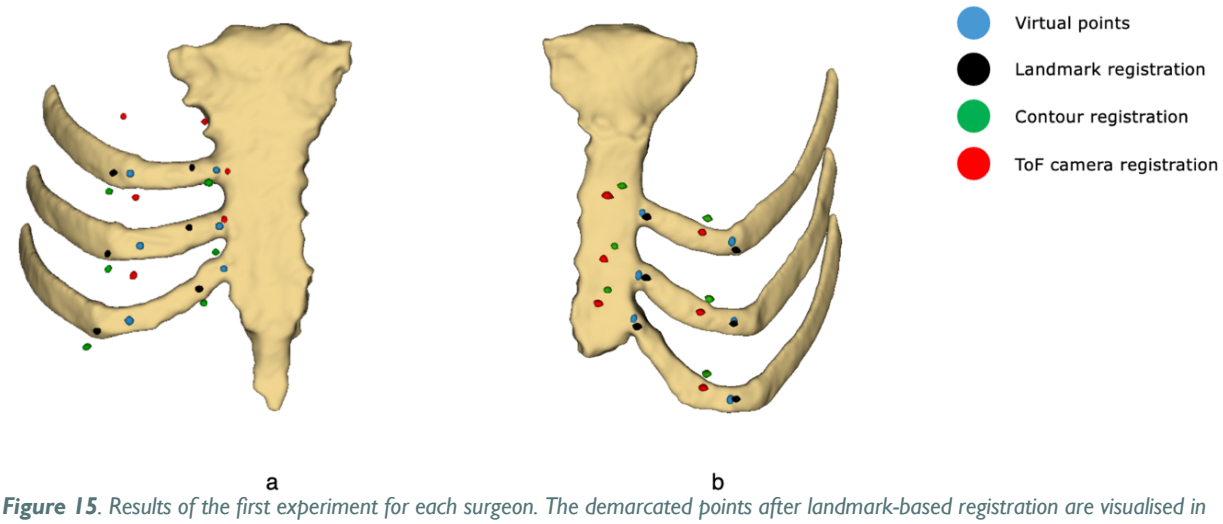

***Figure 15**. Results of the first experiment for each surgeon. The demarcated points after landmark-based registration are visualised in black, the contour registration in green and ToF camera registration in red. The virtual target points are visualised in blue. **a)** Results of Surgeon 1. **b)** Results of Surgeon 2.*

The results of the questionnaire which evaluated the applicability of each registration method are shown in Table 3. In general, both surgeons were satisfied with the ease and speed of all three registration methods. When comparing the results of both surface matching methods, the surgeons do not agree on the projection accuracy and applicability of the methods for chest wall resections. Surgeon 1 indicates that the surface matching methods do not meet the required standards for clinical use. Surgeon 2 is more positive towards their applicability and would use both methods during surgery.

***Table 3**. Evaluation of each registration method for the use of registration pre-incision.*

Statement	Landmark-based registration		Contour registration		ToF camera registration	
	Surgeon 1	*Surgeon 2*	*Surgeon 1*	*Surgeon 2*	*Surgeon 1*	*Surgeon 2*
Registration was quick.	5	4	3	4	4	4
Registration was easy to perform.	5	4	4	5	4	4
Based on my own interpretation of the anatomy, the holographic overlay seemed accurate.	4	4	2	4	1	4
I would use this registration method during surgery (pre-incision)	5	4	1	4	1	4

1 = strongly disagree, 2 = disagree, 3 = neutral, 4 = agree, 5 = strongly agree.

Experiment 2

Figure 24 shows the results of the simulated chest wall resections for each surgeon and each surface matching method. The postoperative model, including the affected ribs and marked tumour, was registered to the preoperative model to give a direct visualisation of the accuracy of resection. Both surgeons were able to locate the tumour in the correct rib by use of each surface matching method. Minor differences can be seen in the length of the tumour segments or the positions of the tumour along the length of the rib. Note that the models do not perfectly align due to differences in segmentation, registration inaccuracies and deformations of the cadavers between the two scans. This makes it difficult to quantify the exact accuracy of the resection.

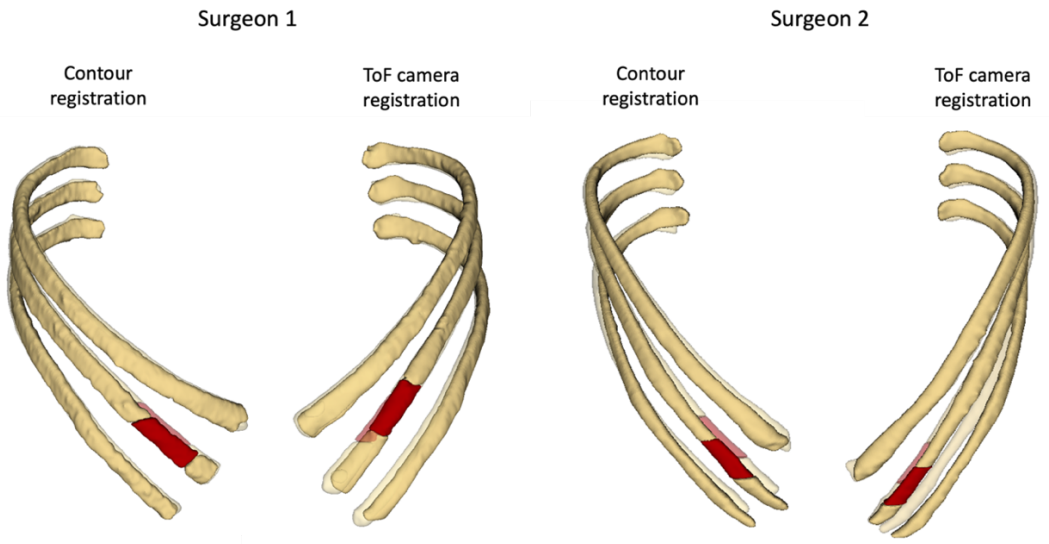

***Figure 16**. Results of the simulated chest wall resection for each surgeon and each surface matching method. The figure shows the postoperative model (non-transparent) registered to the preoperative model (transparent).*

Table 4 and 5 show the results of the questionnaires that were completed after the registration pre-incision and post-incision respectively. When looking at the use of the contour registration method for tumour localisation prior to incision, Surgeon 1 indicated that the use of the HoloLens changed his surgical plan and he planned the resection according to the holographic overlay. Surgeon 2 did not change his surgical plan, as he indicated that he was already confident about the localisation of the rib based on palpation alone. However, the projection of the virtual model did seem accurate and improved his confidence before starting the actual resection.

When looking at the use of the ToF camera registration for tumour localisation pre-incision, Surgeon 1 indicated that the projection seemed accurate and confirmed the tumour localisation based on palpation. For Surgeon 2, the projection was less accurate, and he therefore planned the resection based on palpation alone.

***Table 4.** Evaluation of the surface matching methods for the use of the HoloLens pre-incision.*

Statement	Contour registration		ToF camera registration	
	Surgeon 1	*Surgeon 2*	*Surgeon 1*	*Surgeon 2*
Based on palpation alone, I was confident about the localisation of the rib/tumour.	2	4	2	4
Based on my own interpretation of the anatomy, the holographic overlay seemed accurate.	3	4	5	3
The use of the HoloLens improved my confidence about the localisation of the rib/tumour.	3	4	5	2
I would dare to make surgical decisions based on the projection of the HoloLens.	3	4	5	2
The use of the HoloLens changed my surgical plan.	4	2	3	2

1 = strongly disagree, 2 = disagree, 3 = neutral, 4 = agree, 5 = strongly agree.

When using the HoloLens for registration on the exposed surface of the ribs, the results of the questionnaire in Table 5 show that the ToF camera registration method did not achieve any accurate projections for neither of the surgeons. The contour registration method however, did result in accurate projections of virtual model. Though the surgeons did not change their surgical plan based on this projection, they did indicate that the use of the HoloLens improved their confidence about the tumour localisation post-incision.

Table 5. *Evaluation of the surface matching methods for the use of the HoloLens post-incision.*

Statement	Contour registration		ToF camera registration	
	Surgeon 1	*Surgeon 2*	*Surgeon 1*	*Surgeon 2*
Based on palpation/inspection alone, I was confident about the localisation of the rib/tumour.	4	4	5	4
Based on my own interpretation of the anatomy, the holographic overlay seemed accurate.	4	4	2	2
The use of the HoloLens improved my confidence about the localisation of the rib/tumour.	4	5	2	2
I would dare to make surgical decisions based on the projection of the HoloLens.	4	3	2	1
The use of the HoloLens changed my surgical plan.	2	2	1	1
I would use this registration method during surgery (post-incision).	4	3	1	1

1 = strongly disagree, 2 = disagree, 3 = neutral, 4 = agree, 5 = strongly agree.

General opinion

At the end of the experiments, the surgeons completed one last questionnaire to evaluate on the general use of the HoloLens during chest wall resections (Table 6). Both surgeons agree on the potential of using AR during these resections, though Surgeon 2 is less convinced of this potential than Surgeon 1. Both surgeons have their doubts about the current added value of the HoloLens for the tumour localisation post-incision. They do think that the use of the HoloLens is worth the additional time and steps that are required within the preoperative and intraoperative workflow.

Table 6. *Evaluation of the general use of the HoloLens during chest wall resections.*

Statement	Score	
	Surgeon 1	*Surgeon 2*
I see potential in the use of the HoloLens during chest wall resections.	5	4
The HoloLens has added value in the localisation of the rib/tumour pre-incision.	5	3
The HoloLens has added value in the localisation of the rib/tumour post-incision.	2	3
The use of the HoloLens is worth the additional time and steps prior to surgery (selection of anatomical landmarks, CT scan in operative position etc.).	5	4
The use of the HoloLens is worth the additional time and steps during surgery (time needed for registration, visualisation etc.).	5	4

1 = strongly disagree, 2 = disagree, 3 = neutral, 4 = agree, 5 = strongly agree.

Discussion

This cadaver study evaluated the clinical applicability of the newly developed surface matching methods by two experiments. The first experiment evaluated the ability to locate the correct ribs by performing registration prior to incision. The results show that the conventional landmark-based registration method still resulted in the most accurate holographic overlay for both surgeons. The surgeons were also able to locate the correct ribs by use of the contour registration method, though the hologram was slightly shifted in either the medial or lateral direction. Registration with the ToF camera only seemed sufficient for one of the surgeons.

An aspect that could have affected the results of the surface matching methods is that the cadavers were frozen during the preoperative CT scan. Thawing of the cadavers resulted in slight

tissue deformations between the preoperative CT scan and intraoperative situation. The deformations were mostly seen near the costal cartilage and abdomen, which was close to the selection of the skin used for registration. The results of the surface matching methods could therefore have been negatively affected by these tissue deformations. It is expected that the landmark-based registration was less prone to these deformations, as the landmarks were positioned on rigid surfaces where the deformations were less present, e.g. the sternum and ribs.

Furthermore, as surface matching was performed on a section of the skin that was far away from the sternum, small registration inaccuracies could have had a relatively big effect on misalignments of the hologram. As the landmarks used for landmark-based registration were positioned close to the sternum, this registration method was less prone to this effect. Consequently, this could explain why the two surface matching methods resulted in bigger shifts of the target points than the landmark-based registration method.

Another important aspect that should be considered when looking at the results of the first experiment is that the visualisation in Figure 23 only shows the misalignments of the demarcated points in the horizontal and vertical direction. In reality, there are also differences in the depth direction, as the target points were positioned directly on the sternum while the demarcated points are positioned on the skin. Misalignments in the horizontal and vertical direction are therefore dependent on the user's line of sight. Retrospectively, the exact line of sight is very difficult to quantify, hence it was chosen to visualise the results from an orthogonal point of view to eliminate the errors in the depth direction.

When analysing the results of the first questionnaire (Table 3) we see that both surgeons were satisfied with the ease and speed of each registration method. However, the surgeons disagreed on the accuracy and applicability of the surface matching methods during surgery. This can be explained by the fact that during the experiment of Surgeon 1, there were technical difficulties with the HoloLens-server connection. This had a significant impact on the performance of both surface matching methods, as registrations had to be repeated a considerable amount of times to reach sufficient results and the overall course of the experiment was disrupted. Consequently, this could have biased the answers and registration results of Surgeon 1.

The second experiment investigated the use of both surface matching methods during an actual chest wall resection. The surgeons were able to locate the tumour in the correct rib with use of both surface matching methods. Subsequently, the tumour edges only showed minor shifts in position and size, indicating that the resections were performed quite accurately.

When looking at the questionnaire for registration pre-incision (Table 4), no clear consensus was reached on which surface matching method seemed most accurate. According to Surgeon 1, registration with the ToF camera resulted in an accurate projection of the virtual model. However, the ToF camera registration did not achieve an accurate projection for Surgeon 2. When comparing the results of the contour registration methods, Surgeon 2 indicated that the projection seemed accurate and improved his confidence in localisation. Surgeon 1 doubted the accuracy of the projection, but decided to perform the resection based on the holographic overlay. Eventually, this led to an accurate resection, indicating that the initial projection was probably correct. When combining the results of both experiments for registration pre-incision, we can conclude that the results of the ToF camera registration method were the least consistent and not always sufficient to locate the correct ribs. These inconsistencies might be explained by the fact that the acquired point cloud by the ToF camera includes a large area of the skin. For the thorax, this is area does not contain any explicit curves or edges. Consequently, the ICP algorithm might have multiple local minimal solutions, which leads to different transformation results for each registration procedure. Thus, even though both surface matching methods have proven their ability to achieve sufficient registration accuracies, the contour registration method seems the most consistent and reliable method for registration on the thorax prior to incision.

For registration post-incision, this cadaver study showed that the ToF camera registration was unsuitable for this cause, as registration resulted in an evident misalignment of the virtual model for both surgeons (Appendix E). This was probably due to the fact that the acquired point

cloud contained noise of surrounding tissues or surgical instruments, which negatively affects the accuracy of the ICP algorithm. As was hypothesised, the contour registration method gave better results. It was possible to achieve a sufficient registration accuracy based on the accessible surface of the exposed ribs, which was only a sub-patch of the preoperative reference surface (Appendix E). These results indicate that registration post-incision is feasible with the use of the contour registration method. However, as the projections still showed slight misalignments of the total model (e.g. the tilted sternum in Figure 22c), the surgeons indicated that they see less potential in using the HoloLens for tumour localisation post-incision (Table 6). Nevertheless, they did indicate that the visualisation post-incision could confirm their localisation based on palpation and made the interpretation of the tumour's length or the direction of the cutting planes more intuitive.

Before the results of this cadaver study can be translated to actual paediatric chest wall resections, there are still several aspects that should be considered. First, the experiments were conducted on the thoraxes of adults. As these are bigger than those of paediatric patients, the surface of the skin is less curved. Moreover, due to practical considerations, the cadavers were lying in supine position instead of the lateral decubitus position corresponding to surgery. Consequently, the surface matching methods were mostly performed on the ventral surface of the thorax instead of the lateral curvature of the ribs. As the ventral side of the thorax has a less distinctive curvature than the lateral side, this could have led to worse registration accuracies as the ICP algorithm works best on explicit surface features.[110] Furthermore, by keeping the cadavers in supine position, the differences in the patient's position that normally occur between the preoperative CT scan and intraoperative situation, could not be taken into account during this cadaver study. Consequently, before the results of this cadaver study can be used for the actual implementation of surface matching during surgery, the software should still be tested in a setting that is more in accordance with the real situation. For example, by performing cadaver tests on smaller bodies that can be placed in lateral decubitus position, more pilot tests on patients in the OR, or by testing the software on volunteers.

Subsequently, once the surface matching methods are extensively validated and prove sufficient accuracies in the clinical setting, efforts should be made to improve the surgeons' trust in the AR technology. During the experiments, the surgeons both commented that they do not yet dare to rely on the localisation based on the HoloLens alone. Inconsistent performance of the device, e.g. the technical difficulties that often arise, or the inaccuracies that easily occur, make it difficult to trust the technology at this point. However, they did indicate that the projection of the virtual model, both pre-incision and post-incision, improved their overall confidence in the localisation of the rib and tumour. The surgeons therefore do see the overall potential of using the HoloLens for the intraoperative localisation of chest wall tumours and agree that it is worth the additional steps that are needed in the pre- and intraoperative workflow. Future developments should therefore focus on the improvement of user-friendliness and robustness of the HoloLens applications. By reducing the matter of inconsistencies and inaccuracies, surgeons will become more willing to use the HoloLens during surgery and the potential for the use of AR during chest wall resections can be fully exploited.

Conclusion

This cadaver study proved the feasibility of two surface matching methods for the use of AR during chest wall resections. Both surface matching methods were able to locate the correct rib by registration pre-incision, though the contour registration method was more consistent than the ToF camera registration. For registration post-incision, the ToF camera registration did not prove to be a suitable method. The contour registration did show sufficient accuracies and was able to improve the surgeons' confidence on the intraoperative localisation of the affected rib and tumour. In general, surgeons see the potential of using AR during paediatric chest wall resections and agree that the use of the HoloLens is worth the additional steps and time in the pre- and intraoperative workflow. However, efforts should still be made to improve their trust in the HoloLens in order to fully benefit from its potential.

7. General discussion

The main goal of this thesis was to improve the conventional Augmented Reality system for the surgical localisation of paediatric chest wall tumours. Therefore, two different surface matching methods were compared to the conventional landmark-based registration method by means of their accuracy and applicability in chest wall resections.

The results of this thesis have proven the feasibility of surface matching for the use of AR during paediatric chest wall resections. The comparison of the two different surface acquisition methods on a 3D printed phantom showed that it was possible to reach an accuracy below 1 cm with both methods. For our clinical application, i.e. the localisation of the correct rib, this would be sufficient. The ToF camera registration was the quickest registration method and took less than half a minute on average. Although the contour registration method was significantly slower, its average registration time of less than one and a half minute would also be clinically acceptable.

When testing both surface matching methods in a surgical setting, the cadaver study showed that surgeons were able to locate the correct rib and tumour with use of both methods. In general, contour registration gave more accurate and consistent results than ToF camera registration. As was hypothesized, contour registration also showed most potential for registration post-incision. It was not possible to perform correct registrations on the post-incision surface with use of the ToF camera registration method, probably due to noise of surrounding tissues and surgical instruments inside the acquired point cloud.

When combining the results of the phantom and cadaver study, it can be concluded that contour registration has the overall best potential as a surface matching method within the application of chest wall resections. When using this method for registration pre-incision, it is possible to locate targets with a sufficient accuracy, especially if the operator is a skilled HoloLens user. Furthermore, contour registration can be used to perform registration on the post-incision surface of the ribs and therefore enable additional AR guidance once the skin has been opened.

To our knowledge, this is the first study to investigate the feasibility of surface matching within the surgical application of chest wall resections. Moreover, only a few studies have been published that describe the performance of the same surface matching methods within other surgical fields.

Liebmann et al. (2019) used a similar 3D printed pointer to perform contour registration with the HoloLens for pedicle screw navigation in spinal surgery.[34] They were able to reach an average screw insertion accuracy of 2,77 mm on a 3D printed phantom of the lumbar spine. A similar study was performed by Gu et al. (2021), who used the same contour registration method for holographic guidance in total shoulder arthroplasty.[111] Contour registration was performed on a 3D printed phantom of the glenoid and resulted in an average TRE of 3,25 mm. In both studies, registration was performed by the operating surgeons, but it is not stated whether they were experienced HoloLens users. If we look at the results of the experienced user within our phantom study, the TRE values of the contour registration method are similar to those of Liebmann and Gu et al. However, if we look at our average TRE results, they are slightly lower than those achieved in the aforementioned studies. The high accuracy results of both Liebmann and Gu et al. can possibly be explained by the fact that registration was performed on phantoms with multiple explicit surface features like spinous and transverse processes, or the glenoid cavity and acromion. The ICP algorithm is therefore more likely to achieve a high registration accuracy than on a smooth surface like the thorax.

Only one study exists where the same contour registration method was tested on a human cadaver. Hoch et al. (2020) used the method as described by Liebmann et al. to perform a periacetabular osteotomy of Ganz with AR guidance.[112] An orthopedic surgeon performed contour registration on the exposed pelvic bone and was able to achieve osteotomies with an average accuracy of 6,6 mm based on the holographic overlay of a preoperative planning. As our cadaver experiments had a different set-up where surgeons performed the resection based on

their own interpretation, it is difficult to compare the accuracy results of Hoch et al. with our cadaver study. However, Hoch et al. performed registration mainly on the dorsal side of the ilium, which is a part of the pelvic bone that does not contain very explicit surface features. It is therefore expected that our contour registration method should be able to achieve comparable accuracy results when measuring TRE's values in a similar cadaver experiment.

If we compare the results of our ToF camera registration with literature, studies describe similar accuracy measurements and limitations. A study by Von Haxthausen et al (2021) tested the same ToF camera registration method on a mannequin and found an average shift of 22,3 mm, 35,6 mm and 13,3 mm in the x-, y- and z-direction respectively.[113] Von Haxthausen et al. did not set any limits to the registration surface, causing the acquired point cloud to contain a lot of outliers, for example of the operation table. Consequently, this could have led to the inaccurate registration results.

A study by Gsaxner et al. (2019) investigated ToF camera registration on the face.[114] Accuracy measurements on eight phantoms and one human subject showed an average TRE of 9,2 mm. Their results are slightly lower than the results of our phantom study. This can possibly be explained by the fact that Gsaxner et al. used a fully automated ICP algorithm that circumvented the initial alignment step. Errors in this alignment step could have caused the algorithm to get trapped in local minima, hereby resulting in worse accuracy results.

The previously mentioned study by Gu et al. also investigated the accuracy of ToF camera registration on 3D printed phantoms of the glenoid.[111] They tested the registration method in a setting where the phantom was either fully exposed or partly obstructed, to mimic the intraoperative situation of total shoulder arthroplasty. Gu et al. found that the registration results on a partly obstructed phantom were insufficient for clinical use, which is in accordance with our findings when using ToF camera registration on the post-incision surface. When testing the ToF camera registration on a fully exposed phantom, Gu et al. achieved a TRE of 9,28 mm, which was mainly caused by a systematic error in the depth direction. They found the ToF camera offset of approximately 1 cm to arise on the 3D printed material as on a porcine specimen. Their results are therefore in accordance with our findings and support the potential of contour registration over ToF camera registration for the use of AR in surgical settings.

When interpreting all results of this thesis for the actual clinical applicability of surface matching during chest wall resections, there are several limitations that should be considered. Firstly, the phantom study did not allow a fair comparison between the conventional landmark-based registration and both surface matching methods. As the landmark-based registration was performed on a rigid panel with pivots, registration could be performed very precisely, and the user-dependent errors that normally arise in the clinical setting were eliminated. This was not the case for both surface matching methods, where results were still dependent on variable factors like the user's HoloLens skills or line-of-sight. Consequently, the phantom study suggests that both surface matching methods are less accurate than the conventional registration method, but these results cannot be generalized to the actual clinical setting. The only way to make a fair comparison between the three registration methods, is to implement them all during actual chest wall resections. Subsequently, all methods can be tested in the OR and the localisation results of the surface matching methods can be compared to the conventional method. Eventually, these experiences will have to point out which registration method leads to the most accurate localisation of the affected ribs according to the surgeons' interpretations.

Secondly, though the cadaver study gives a good impression of the applicability of surface matching during chest wall resections, there were still several factors that differed from the actual situation in the OR. The use of frozen cadavers that only consisted of the thorax made it impossible to place the bodies in lateral decubitus position during the preoperative CT scan, hence it was chosen to keep the cadavers in supine position throughout the whole experiment. The position differences that normally occur in the clinical setting could therefore not be taken into account. However, these differences can have a significant effect on the registration accuracy, and it is thus important to evaluate the performance of the registration methods when slight thorax

deformations might have occurred between the preoperative CT and intraoperative situation. It is expected that landmark-based registration is more prone to these inaccuracies than the surface matching methods, as registration is performed on only a small number of points. If there is a mismatch between some of these points, this can have a relatively big effect on the overall registration result. With surface matching, registration is performed on a large point cloud, and it is thus expected that mismatches will lead to a less significant effect.

The supine position of the cadavers also caused the registration surface to be more on the ventral side of the thorax than on the lateral side which would normally be used during surgery. The ventral side of the thorax is less curved and could thus have led to less accurate registration results for the surface matching methods. Future studies should therefore focus on comparing the registration methods in an even more realistic setting. For example, by using thawed full body cadavers that can be placed in lateral decubitus position, or on volunteers or actual patients in the OR. This way the effect of thorax deformations can be considered, and registration can be performed on the lateral side of the thorax.

Lastly, the HoloLens application that was used for the surface matching methods was still under construction. Consequently, we encountered a lot of technical difficulties (e.g. failed server connection, or incorrect tracking of the pointer) during all experiments. This could have negatively affected the registration results, but also the general opinion of the surgeons towards the use of surface matching during chest wall resections. Currently, surgeons indicate that they do not yet dare to make surgical decisions based on the HoloLens alone, due to frequent malfunctioning of the device and inconsistent accuracy results. However, the results of this thesis suggest that contour registration could solve parts of these shortcomings. Once the surgeons become more experienced HoloLens users, contour registration could serve as an accurate and consistent registration method that is less prone to user-dependent errors and deformations of the thorax. Nevertheless, the application's user-friendliness, robustness, and HoloLens-server connection should still be improved before the application can be clinically implemented.

Additionally, efforts should be made to restore the surgeons' trust in using the HoloLens for surgical localisations. Without this trust, surgeons will still use additional and invasive imaging techniques such as thoracoscopy to confirm the location of the tumour, hereby undermining the potential of AR. In the future, educating and training surgeons to use the HoloLens more intensively could solve parts of this challenge. Surgeons could be trained by performing the registration on realistic phantoms, or by playing AR games to improve their general HoloLens skills. Furthermore, the frequency with which they use the HoloLens could be increased by implementing the technique in other surgical procedures, such as orthopedic, maxillo-facial, or nephron-sparing surgery. According to the results of our phantom study, skilled surgeons should be able to achieve high accuracy results with the contour registration method. Implementing this method in the standard workflow for chest wall resections will eventually prove the accuracy of contour registration in actual clinical practice. Ultimately, if this is sufficient, surgeons will hopefully dare to rely on the tumour localisation based on the HoloLens alone, without needing additional and invasive intraoperative imaging techniques.

The implementation of contour registration in the workflow for chest wall resections will be similar to the conventional AR system. During the pre-operative CT scan, the patient should still be positioned according to surgery, but it would no longer be necessary to select anatomical landmarks on the patient's skin. A technical physician can then prepare the preoperative 3D and should collaborate with the operating surgeon to determine which surfaces will be accessible for registration both pre- and post-incision. Subsequently, the technical physician will prepare the HoloLens application and provide the technical support during surgery. Like the conventional landmark-based registration, registration pre-incision can be performed before the sterile field is in place. Subsequently, the holographic overlay will enable a quick and non-invasive localisation of the affected ribs without the need of additional imaging techniques. For registration post-incision, contour registration can serve as an additional confirmation of the tumour localisation to improve the surgeons' confidence before starting the actual resection. Consequently, the use of AR can facilitate surgical decision making and reduce the overall complexity and time-consuming process of intraoperative tumour localisation during chest wall resections.

Conclusion

This thesis explored the feasibility of surface matching for the use of AR during paediatric chest wall resections. Two surface acquisition methods were compared to the conventional landmark-based registration method through a phantom and cadaver study. The phantom study showed that it was feasible to perform surface matching on both pre-incision and post-incision surfaces of the thorax, i.e. on the skin and exposed ribs respectively. Both surface matching methods showed clinically acceptable registration times and sufficient registration accuracies below 1 cm.

To test the surface matching methods in a more realistic setting, a cadaver study was performed which investigated the applicability of both methods during a simulated chest wall resection. Surgeons were able to locate the correct rib with both surface matching methods. However, the ToF camera registration showed the least consistent results and proved to be unsuitable for registration on the post-incision surface of the exposed ribs. Consequently, combining all results of this thesis, contour registration shows the most potential as a surface matching method during chest wall resections.

Before the contour registration method can be implemented during chest wall resections, future studies should evaluate the registration performance in even more realistic settings, for example on smaller cadavers that can be put in lateral decubitus position, volunteers, or patients in the OR. Subsequently, efforts should be made to improve the user-friendliness and robustness of the HoloLens application, hereby restoring the surgeons' trust in the technique. This should improve the willingness of surgeons to use AR during surgery and ultimately lead to better HoloLens skills and registration accuracies. Ultimately, the use of AR can facilitate surgical decision making and improve intraoperative tumour localisation during paediatric chest wall resections.

References

1. Rubin, E. & Reisner, H. M. *Essentials of Rubin's Pathology*. (Wolters Kluwer Health, 2011).
2. Desai, S. S. & Jambhekar, N. A. Pathology of Ewing's sarcoma/PNET: Current opinion and emerging concepts. *Indian Journal of Orthopaedics* **44**, 363 (2010).
3. Prinses Máxima Centrum. Ewing-sarcoom. *Zorg* https://zorg.prinsesmaximacentrum.nl/nl/diagnose/ewing-sarcoom.
4. Durer, S. & Shaikh, H. Ewing Sarcoma. in *StatPearls* (StatPearls Publishing, 2023).
5. Esiashvili, N., Goodman, M. & Marcus, R. B. Changes in Incidence and Survival of Ewing Sarcoma Patients Over the Past 3 Decades: Surveillance Epidemiology and End Results Data. *Journal of Pediatric Hematology/Oncology* **30**, 425–430 (2008).
6. Zöllner, S. K. *et al.* Ewing Sarcoma—Diagnosis, Treatment, Clinical Challenges and Future Perspectives. *J Clin Med* **10**, 1685 (2021).
7. de Alava, E. Ewing Sarcoma, an Update on Molecular Pathology with Therapeutic Implications. *Surgical Pathology Clinics* **10**, 575–585 (2017).
8. Hamilton, S. N., Carlson, R., Hasan, H., Rassekh, S. R. & Goddard, K. Long-term Outcomes and Complications in Pediatric Ewing Sarcoma. *American Journal of Clinical Oncology* **40**, 423 (2017).
9. Ho, V., de Heus, E. & de Peuter, R. *Sarcomenzorg in Nederland: overzicht van de Nederlandse Kankerregistratie over de periode 2009-2018*. https://iknl.nl/getmedia/b2538482-8e79-40d5-a4ff-90e4b1e54838/Rapport-Sarcomenzorg-in-Nederland_2020_IKNL_NKR.pdf.
10. Siegel, R. L., Miller, K. D., Fuchs, H. E. & Jemal, A. Cancer statistics, 2022. *CA: A Cancer Journal for Clinicians* **72**, 7–33 (2022).
11. EURO EWING Study Group. *EWING 2008 Protocol*. https://www.skion.nl/workspace/uploads/C2--EWING2008_Protocol_Versie-2-1_01-03-2018_1.pdf (2018).
12. Lopez, C. *et al.* Outcomes of chest wall resections in pediatric sarcoma patients. *Journal of Pediatric Surgery* **52**, 109–114 (2017).
13. Bosma, S. E. *et al.* What Do We Know about Survival in Skeletally Premature Children Aged 0 to 10 Years with Ewing Sarcoma? A Multicenter 10-Year Follow-Up Study in 60 Patients. *Cancers* **14**, (2022).

14. Glotzbecker, M. P., Gold, M., Puder, M. & Hresko, M. T. Scoliosis after chest wall resection. *Journal of Children's Orthopaedics* **7**, 301–307 (2013).
15. Lelkes, V. M., Jones, K. B. & Groundland, J. S. Chest Wall Resection for Sarcoma: A Surgical Technique and Case Series. *Operative Techniques in Orthopaedics* **30**, 100801 (2020).
16. Basharkhah, A. *et al.* Interdisciplinary Radical "En-Bloc" Resection of Ewing Sarcoma of the Chest Wall and Simultaneous Chest Wall Repair Achieves Excellent Long-Term Survival in Children and Adolescents. *Frontiers in Pediatrics* **9**, (2021).
17. Spijkerboer, K. G. P. To improve patient-specific visualisation during the surgical treatment of chest wall Ewing sarcomas in pediatric oncology using 3D patient-specific models and augmented reality. *Thesis* (2022).
18. Meulstee, J. W. *et al.* Toward Holographic-Guided Surgery. *Surgical Innovation* **26**, 86–94 (2019).
19. Yoon, J. W. *et al.* Augmented reality for the surgeon: Systematic review. *International Journal of Medical Robotics and Computer Assisted Surgery* **14**, 1–13 (2018).
20. Zhao, Z. *et al.* Augmented reality technology in image-guided therapy: State-of-the-art review. *Proceedings of the Institution of Mechanical Engineers, Part H: Journal of Engineering in Medicine* **235**, 1386–1398 (2021).
21. Badiali, G. *et al.* Review on Augmented Reality in Oral and Cranio-Maxillofacial Surgery: Toward 'Surgery-Specific' Head-Up Displays. *IEEE Access* **8**, 59015–59028 (2020).
22. Doughty, M., Ghugre, N. R. & Wright, G. A. Augmenting Performance: A Systematic Review of Optical See-Through Head-Mounted Displays in Surgery. *Journal of Imaging* **8**, 203 (2022).
23. Vávra, P. *et al.* Recent Development of Augmented Reality in Surgery: A Review. *Journal of Healthcare Engineering* **2017**, (2017).
24. Dennler, C. *et al.* Augmented reality in the operating room: a clinical feasibility study. *BMC musculoskeletal disorders* **22**, (2021).
25. Fida, B., Cutolo, F., di Franco, G., Ferrari, M. & Ferrari, V. Augmented reality in open surgery. *Updates in Surgery* **70**, 389–400 (2018).
26. Bussink, T., Maal, T., Meulstee, J. & Xi, T. Augmented reality guided condylectomy. *British Journal of Oral and Maxillofacial Surgery* **60**, 991–993 (2022).

27. Spijkerboer, K. G. P., Fitski, M., Siepel, F. J., van de Ven, C. P. & van der Steeg, A. F. W. Augmented reality-guided localization of a chest wall tumor in a pediatric patient. *European Journal of Cancer* **170**, 103–105 (2022).
28. Fan, Y., Jiang, D., Wang, M. & Song, Z. A new markerless patient-to-image registration method using a portable 3D scanner. *Medical Physics* **41**, 101910 (2014).
29. Dong, Y., Zhang, C., Ji, D., Wang, M. & Song, Z. Regional-surface-based registration for image-guided neurosurgery: effects of scan modes on registration accuracy. *Int J CARS* **14**, 1303–1315 (2019).
30. Fan, Y., Yao, X. & Xu, X. A robust automated surface-matching registration method for neuronavigation. *Medical Physics* **47**, 2755–2767 (2020).
31. Audette, M. A., Ferrie, F. P. & Peters, T. M. An algorithmic overview of surface registration techniques for medical imaging. *Medical Image Analysis* **4**, 201–217 (2000).
32. Wu, M.-L., Chien, J.-C., Wu, C.-T. & Lee, J.-D. An Augmented Reality System Using Improved-Iterative Closest Point Algorithm for On-Patient Medical Image Visualisation. *Sensors (Basel)* **18**, 2505 (2018).
33. Ohba, S., Yoshimura, H., Ishimaru, K., Awara, K. & Sano, K. Application of a real-time three-dimensional navigation system to various oral and maxillofacial surgical procedures. *Odontology* **103**, 360–366 (2015).
34. Liebmann, F. *et al.* Pedicle screw navigation using surface digitization on the Microsoft HoloLens. *International Journal of Computer Assisted Radiology and Surgery* **14**, 1157–1165 (2019).
35. Ewing, J. Diffuse Endothelioma of Bone. *Proceedings of the New York Pathological Society* 17–24 (1921).
36. Cripe, T. P. Ewing Sarcoma: An Eponym Window to History. *Sarcoma* **2011**, e457532 (2010).
37. Sole, A. *et al.* Unraveling Ewing Sarcoma Tumorigenesis Originating from Patient-Derived Mesenchymal Stem Cells. *Cancer Research* **81**, 4994–5006 (2021).
38. Lin, P. P., Wang, Y. & Lozano, G. Mesenchymal Stem Cells and the Origin of Ewing's Sarcoma. *Sarcoma* **2011**, 276463 (2011).
39. Khan, S. *et al.* Incidence of Ewing's Sarcoma in Different Age Groups, Their Associated Features, and Its Correlation With Primary Care Interval. *Cureus* **13**, e13986.
40. Goedhart, L. M. *et al.* Bone sarcoma incidence in the Netherlands. *Cancer Epidemiology* **60**, 31–38 (2019).

41. Kridis, W. B. *et al.* A Review of Ewing Sarcoma Treatment: Is it Still a Subject of Debate? *Reviews on Recent Clinical Trials* **12**, 19–23.
42. Duchman, K. R., Gao, Y. & Miller, B. J. Prognostic factors for survival in patients with Ewing's sarcoma using the surveillance, epidemiology, and end results (SEER) program database. *Cancer Epidemiology* **39**, 189–195 (2015).
43. Bedetti, B. *et al.* Local Control in Ewing Sarcoma of the Chest Wall: Results of the EURO-EWING 99 Trial. *Ann Surg Oncol* **22**, 2853–2859 (2015).
44. Biermann, J. S. *et al.* NCCN Guidelines Insights: Bone Cancer, Version 2.2017. *Journal of the National Comprehensive Cancer Network* **15**, 155–167 (2017).
45. Puchalski, A. Ewing sarcoma family of tumors. *Journal of Diagnostic Medical Sonography* **26**, 238–244 (2010).
46. Vadera, S. & Gaillard, F. Ewing sarcoma. *Radiopaedia.org* (2009) doi:10.53347/RID-7852.
47. Murphey, M. D. *et al.* From the Radiologic Pathology Archives: Ewing Sarcoma Family of Tumors: Radiologic-Pathologic Correlation. *RadioGraphics* **33**, 803–831 (2013).
48. Burchill, S. A. Ewing's sarcoma: diagnostic, prognostic, and therapeutic implications of molecular abnormalities. *Journal of Clinical Pathology* **56**, 96–102 (2003).
49. Anderton, J. *et al.* International randomised controlled trial for the treatment of newly diagnosed EWING sarcoma family of tumours – EURO EWING 2012 Protocol. *Trials* **21**, 96 (2020).
50. Interim Ewing info (versie 1). https://prinsesmaxima.iprova.nl/Portal/#/document/d9e0a816-4b82-4389-9e43-bed2d30701b2.
51. Koch, R. *et al.* High-Dose Treosulfan and Melphalan as Consolidation Therapy Versus Standard Therapy for High-Risk (Metastatic) Ewing Sarcoma. *JCO* **40**, 2307–2320 (2022).
52. Saltsman, J. A. *et al.* Survival and Scoliosis Following Resection of Chest Wall Tumors in Children and Adolescents: A Single-center Retrospective Analysis. *Annals of surgery* **274**, e167–e173 (2021).
53. Harris, C. J. *et al.* Implications of Tumor Characteristics and Treatment Modality on Local Recurrence and Functional Outcomes in Children With Chest Wall Sarcoma: A Pediatric Surgical Oncology Research Collaborative Study. *Annals of Surgery* **276**, e969 (2022).
54. Arun, P. S. Types of Surgical Resection of Tumors | Bone and Spine. https://boneandspine.com/types-of-surgical-resection-of-tumors/ (2017).

55. Mesko, N. W., Bribriesco, A. C. & Raymond, D. P. Surgical Management of Chest Wall Sarcoma. *Surgical Oncology Clinics of North America* **29**, 655–672 (2020).
56. Sandler, G. & Hayes-Jordan, A. Chest wall reconstruction after tumor resection. *Seminars in Pediatric Surgery* **27**, 200–206 (2018).
57. Theodorou, C. M., Lawrence, Y. S. & Brown, E. G. Chest wall reconstruction in pediatric patients with chest wall tumors: A systematic review. *Journal of Pediatric Surgery* (2022) doi:10.1016/j.jpedsurg.2022.11.008.
58. Fuchs, B., Valenzuela, R. G., Inwards, C., Sim, F. H. & Rock, M. G. Complications in long-term survivors of Ewing sarcoma. *Cancer* **98**, 2687–2692 (2003).
59. Scalabre, A. *et al.* Prognostic Risk Factors for the Development of Scoliosis After Chest Wall Resection for Malignant Tumors in Children. *The Journal of Bone & Joint Surgery* **96**, 10 (2014).
60. Seitz, G. *et al.* Treatment and outcome of patients with thoracic tumors of the Ewing sarcoma family: A report from the Cooperative Weichteilsarkom Studiengruppe CWS-81, -86, -91, -96, and -2002P trials. *Pediatric Blood & Cancer* **66**, e27537 (2019).
61. Ryan, T. D., Nagarajan, R. & Godown, J. Cardiovascular Toxicities in Pediatric Cancer Survivors. *Cardiology Clinics* **37**, 533–544 (2019).
62. Bishop, M. W. *et al.* Cumulative Burden of Chronic Health Conditions in Adult Survivors of Osteosarcoma and Ewing Sarcoma: A Report from the St. Jude Lifetime Cohort Study. *Cancer Epidemiology, Biomarkers & Prevention* **29**, 1627–1638 (2020).
63. Kadan-Lottick, N. S. *et al.* Patient-reported neurocognitive function in adult survivors of childhood and adolescent osteosarcoma and Ewing sarcoma. *J Cancer Surviv* **17**, 1238–1250 (2023).
64. Ranft, A. *et al.* Quality of Survivorship in a Rare Disease: Clinicofunctional Outcome and Physical Activity in an Observational Cohort Study of 618 Long-Term Survivors of Ewing Sarcoma. *JCO* **35**, 1704–1712 (2017).
65. Stish, B. J., Ahmed, S. K., Rose, P. S., Arndt, C. A. & Laack, N. N. Patient-Reported Functional and Quality of Life Outcomes in a Large Cohort of Long-Term Survivors of Ewing Sarcoma. *Pediatric Blood & Cancer* **62**, 2189–2196 (2015).
66. Sprangers, M. A. G. & Schwartz, C. E. Integrating response shift into health-related quality of life research: a theoretical model. *Social Science & Medicine* **48**, 1507–1515 (1999).

67. Albrecht, G. L. & Devlieger, P. J. The disability paradox: high quality of life against all odds. *Social Science & Medicine* **48**, 977–988 (1999).
68. Mekni, M. & Lemieux, A. Augmented Reality: Applications, Challenges and Future Trends.
69. Birlo, M., Edwards, P. J. E., Clarkson, M. & Stoyanov, D. Utility of optical see-through head mounted displays in augmented reality-assisted surgery: A systematic review. *Medical Image Analysis* **77**, 102361 (2022).
70. Cutolo, F., Cattari, N., Fontana, U. & Ferrari, V. Optical See-Through Head-Mounted Displays With Short Focal Distance: Conditions for Mitigating Parallax-Related Registration Error. *Frontiers in Robotics and AI* **7**, (2020).
71. Barsom, E. Z., Graafland, M. & Schijven, M. P. Systematic review on the effectiveness of augmented reality applications in medical training. *Surg Endosc* **30**, 4174–4183 (2016).
72. Image Registration - an overview | ScienceDirect Topics. https://www-sciencedirect-com.ezproxy2.utwente.nl/topics/neuroscience/image-registration.
73. van der Heijden, F. Surgical Navigation Techniques [Syllabus]. (2022).
74. Alam, F., Rahman, S. U., Ullah, S. & Gulati, K. Medical image registration in image guided surgery: Issues, challenges and research opportunities. *Biocybernetics and Biomedical Engineering* **38**, 71–89 (2018).
75. Maintz, J. B. A. & Viergever, M. A. An Overview of Medical Image Registration Methods. in (Imaging Science Department, Universiteit Utrecht, 1998).
76. Olesch, J., Papenberg, N., Lange, T., Conrad, M. & Fischer, B. Matching CT and ultrasound data of the liver by landmark constrained image registration. in vol. 7261 (2009).
77. Sun, H. *et al.* Image-guided endoscopic navigation for the precise resection of a mandibular condylar osteochondroma. *Journal of Craniofacial Surgery* **24**, e573–e579 (2013).
78. Sadeghi-Niaraki, A. & Choi, S.-M. A Survey of Marker-Less Tracking and Registration Techniques for Health & Environmental Applications to Augmented Reality and Ubiquitous Geospatial Information Systems. *Sensors* (2020) doi:10.3390/s20102997.
79. de Geer, A. F. *et al.* Registration methods for surgical navigation of the mandible: a systematic review. *International Journal of Oral and Maxillofacial Surgery* **51**, 1318–1329 (2022).
80. Kabsch algorithm. *Wikipedia* (2023).

81. Fabry, T., Smeets, D. & Vandermeulen, D. Surface representations for 3D face recognition. in (2010). doi:10.5772/8951.
82. Xie, Y., Zeng, R., Yan, J., Yan, T. & Tan, J. Introducing surface-to-surface matching technique to evaluate mandibular symmetry: A retrospective study. *Heliyon* **8**, e09914 (2022).
83. Su, S.-T., Ho, M.-C., Yen, J.-Y. & Chen, Y.-Y. Featured Surface Matching Method for Liver Image Registration. *IEEE Access* **8**, 59723–59731 (2020).
84. Willems, P., Berkelbach van der Sprenkel, J. W., Tulleken, C. A. F., Viergever, M. A. & Taphoorn, M. J. B. Neuronavigation and surgery of intracerebral tumours. *Journal of neurology* **253**, 1123–36 (2006).
85. Besl, P. J. & McKay, N. D. A Method for Registration of 3-D Shapes. *IEEE Transactions on Pattern Analysis and Machine Intelligence* **14**, 239–256 (1992).
86. Iterative Closest Point Algorithm - an overview | ScienceDirect Topics. https://www-sciencedirect-com.ezproxy2.utwente.nl/topics/engineering/iterative-closest-point-algorithm.
87. Bærentzen, J. A., Gravesen, J., Anton, F. & Aanæs, H. 3D Surface Registration via Iterative Closest Point (ICP). *Guide to Computational Geometry Processing* 263–275 (2012) doi:10.1007/978-1-4471-4075-7_15.
88. Stachniss, C. ICP & Point Cloud Registration - Part 2: Unknown Data Association. in *Mobile Sensing And Robotics 2* (2021).
89. Simpson, A. L. *et al.* Comparison Study of Intraoperative Surface Acquisition Methods for Surgical Navigation. *IEEE Transactions on Biomedical Engineering* **60**, 1090–1099 (2013).
90. de Boutray, M. *et al.* Fibular registration using surface matching in navigation-guided osteotomies: a proof of concept study on 3D-printed models. *International Journal of Computer Assisted Radiology and Surgery* **17**, 1321–1331 (2022).
91. Shamir, R. R., Freiman, M., Joskowicz, L., Spektor, S. & Shoshan, Y. Surface-based facial scan registration in neuronavigation procedures: a clinical study: Clinical article. *Journal of Neurosurgery* **111**, 1201–1206 (2009).
92. Liu, H. & Baena, F. R. Y. Automatic Markerless Registration and Tracking of the Bone for Computer-Assisted Orthopaedic Surgery. *IEEE Access* **8**, 42010–42020 (2020).
93. Li, W. *et al.* An incremental registration method for endoscopic sinus and skull base surgery navigation: From phantom study to clinical trials. *Medical Physics* **50**, 226–239 (2023).

94. Fedorov, A. *et al.* 3D Slicer as an image computing platform for the Quantitative Imaging Network. *Magnetic Resonance Imaging* **30**, 1323–1341 (2012).
95. Zhou, Q.-Y., Park, J. & Koltun, V. Open3D: A Modern Library for 3D Data Processing. *arXiv:1801.09847* (2018).
96. Segal, A., Hähnel, D. & Thrun, S. Generalized-ICP. in (2009).
97. Rusinkiewicz, S. & Levoy, M. Efficient variants of the ICP algorithm [Conference Paper]. in *Proceedings Third International Conference on 3-D Digital Imaging and Modeling* 145–152 (IEEE Comput. Soc, 2001). doi:10.1109/IM.2001.924423.
98. Low, K.-L. Linear Least-Squares Optimization for Point-to-Plane ICP Surface Registration. (2004).
99. Chen, Y. & Medioni, G. Object modelling by registration of multiple range images. *Image and Vision Computing* **10**, 145–155 (1992).
100. thetuvix. Using Vuforia with Unity - Mixed Reality. https://learn.microsoft.com/en-us/windows/mixed-reality/develop/unity/vuforia-development-overview (2021).
101. Hansard, M., Lee, S., Choi, O. & Horaud, R. *Time-of-Flight Cameras: Principles, Methods and Applications*. vol. 1 (Springer London, 2012).
102. Gokturk, S. B., Yalcin, H. & Bamji, C. A Time-Of-Flight Depth Sensor - System Description, Issues and Solutions. in *2004 Conference on Computer Vision and Pattern Recognition Workshop* 35–35 (2004). doi:10.1109/CVPR.2004.291.
103. He, Y., Liang, B., Zou, Y., He, J. & Yang, J. Depth Errors Analysis and Correction for Time-of-Flight (ToF) Cameras. *Sensors (Basel)* **17**, 92 (2017).
104. Ungureanu, D. *et al.* HoloLens 2 Research Mode as a Tool for Computer Vision Research. *ArXiv* (2020).
105. Kinnen, T., Blut, C., Effkemann, C. & Blankenback, J. Thermal reality capturing with the Microsoft HoloLens 2 for energy system analysis. *Energy and Buildings* **288**, 113020 (2023).
106. vtieto. HoloLens Research Mode - Mixed Reality. https://learn.microsoft.com/en-us/windows/mixed-reality/develop/advanced-concepts/research-mode (2022).
107. Simulator coordinate system - LGSVL Simulator. https://www.svlsimulator.com/docs/archive/2020.06/simulator-coordinate-system/.
108. Fedorov, A. *et al.* 3D Slicer as an image computing platform for the Quantitative Imaging Network. *Magnetic Resonance Imaging* **30**, 1323–1341 (2012).

109. Norrdine, A. An Algebraic Solution to the Multilateration Problem. *International Conference on Indoor Positioning and Indoor Navigation* (2015) doi:10.13140/RG.2.1.1681.3602.

110. Bærentzen, J. A., Gravesen, J., Anton, F. & Aanæs, H. 3D Surface Registration via Iterative Closest Point (ICP). in *Guide to Computational Geometry Processing: Foundations, Algorithms, and Methods* (eds. Bærentzen, J. A., Gravesen, J., Anton, F. & Aanæs, H.) 263–275 (Springer, 2012). doi:10.1007/978-1-4471-4075-7_15.

111. Gu, W., Shah, K., Knopf, J., Navab, N. & Unberath, M. Feasibility of image-based augmented reality guidance of total shoulder arthroplasty using microsoft HoloLens 1. *Computer Methods in Biomechanics and Biomedical Engineering: Imaging and Visualisation* **9**, 261–270 (2021).

112. Hoch, A. *et al.* Augmented Reality Based Surgical Navigation of the Periacetabular Osteotomy of Ganz – A Pilot Cadaveric Study. in *New Trends in Medical and Service Robotics* (eds. Rauter, G. et al.) 192–201 (Springer International Publishing, 2021). doi:10.1007/978-3-030-58104-6_22.

113. Von Haxthausen, F., Chen, Y. & Ernst, F. Superimposing holograms on real world objects using HoloLens 2 and its depth camera. *Current Directions in Biomedical Engineering* **7**, 111–115 (2021).

114. Gsaxner, C., Pepe, A., Wallner, J., Schmalstieg, D. & Egger, J. Markerless Image-to-Face Registration for Untethered Augmented Reality in Head and Neck Surgery. in *Medical Image Computing and Computer Assisted Intervention – MICCAI 2019* (eds. Shen, D. et al.) 236–244 (Springer International Publishing, 2019). doi:10.1007/978-3-030-32254-0_27.

Appendix A

Unity TCP client script

Confidential.

Appendix B

Python TCP server script

Confidential.

Appendix C

Trilateration calculations

```
@author: remivanderwoude


import open3d as o3d
import numpy as np
import pandas as pd
import math

excel_path = r"\\Mac\Home\Documents\M3 - PMC\Fantoom
tests\Measurements\Accuracy_prot2_ob2\prot2_distances_230712_r5_ob2.xlsx"
excel_writer = r"\\Mac\Home\Documents\M3 - PMC\Fantoom
tests\Measurements\Accuracy_prot2_ob2\prot2_positions_230712_r5_ob2.xlsx"
phantom = 1 # 1 = pre-incision, 2 = post-incision"
sheetname = 0 #0: Landmark registration - 1: Contour registration - 2: ToF registration

distances = pd.read_excel(excel_path, sheetname, index_col=0)

if phantom == 1:
    beacon1 = np.array([-88.451, -99.979, -55.677])
    beacon2 = np.array([-31.302, -126.128, -36.370])
    beacon3 = np.array([-3.198, -115.480, -54.818])
    beacon4 = np.array([-34.474, -118.762, -72.748])
    beacon5 = np.array([-35.947, -112.562, -98.289])
    beacons = np.stack((beacon1,beacon2,beacon3,beacon4,beacon5))

    target1 = np.array([-74.864, -115.943, -28.205])
    target2 = np.array([-74.864, -110.662, -60.600])
    target3 = np.array([-74.864, -105.500, -92.995])
    target4 = np.array([-42.469, -127.580, -28.205])
    target5 = np.array([-42.469, -121.910, -60.600])
    target6 = np.array([-42.469, -115.210, -92.995])
    target7 = np.array([-10.074, -125.130, -28.205])
    target8 = np.array([-10.074, -117.650, -60.600])
    target9 = np.array([-10.074, -108.690, -92.995])
    targets = np.stack((target1, target2, target3, target4, target5, target6, target7,
target8, target9))

if phantom == 2:
    beacon1 = np.array([-77.997, -89.031, -54.581])
    beacon2 = np.array([-32.150, -103.805, -33.477])
    beacon3 = np.array([-8.371, -95.829, -51.629])
    beacon4 = np.array([-36.036, -99.654, -67.531])
    beacon5 = np.array([-37.428, -96.808, -93.652])
    beacons = np.stack((beacon1,beacon2,beacon3,beacon4,beacon5))

    target1 = np.array([-65.760, -97.870, -36.000])
    target2 = np.array([-65.760, -94.500, -63.495])
    target3 = np.array([-65.760, -94.350, -90.990])
    target4 = np.array([-38.265, -105.560, -36.000])
    target5 = np.array([-38.265, -103.110, -63.495])
    target6 = np.array([-38.265, -98.400, -90.990])
    target7 = np.array([-10.770, -99.950, -36.000])
    target8 = np.array([-10.770, -96.860, -63.495])
    target9 = np.array([-10.770, -92.630, -90.990])
    targets = np.stack((target1, target2, target3, target4, target5, target6, target7,
target8, target9))

positions = pd.DataFrame(columns=['x','y','z','RMS'])
```

```
for target in range(9):
    print("target =", target+1)
    dist_target = distances.iloc[target,:]
    dist_target_np = dist_target.to_numpy()
    index1 = dist_target_np.argsort()[0]
    index2 = dist_target_np.argsort()[1]
    index3 = dist_target_np.argsort()[2]
    index4 = dist_target_np.argsort()[3]
    dist_sorted = dist_target.sort_values()

    # d1 = dist_sorted.iloc[0]
    # d2 = dist_sorted.iloc[1]
    # d3 = dist_sorted.iloc[2]
    # d4 = dist_sorted.iloc[3]

    # P1 = beacons[index1,:]
    # P2 = beacons[index2,:]
    # P3 = beacons[index3,:]
    # P4 = beacons[index4,:]

    P1 = beacons[0,:]
    P2 = beacons[1,:]
    P3 = beacons[2,:]
    P4 = beacons[3,:]

    d1 = dist_target_np[0]
    d2 = dist_target_np[1]
    d3 = dist_target_np[2]
    d4 = dist_target_np[4]

    def trilateration(P1, P2, P3, P4, r1, r2, r3, r4):

        p1 = np.array([0, 0, 0])
        p2 = np.array([P2[0] - P1[0], P2[1] - P1[1], P2[2] - P1[2]])
        p3 = np.array([P3[0] - P1[0], P3[1] - P1[1], P3[2] - P1[2]])
        v1 = p2 - p1
        v2 = p3 - p1

        Xn = (v1)/np.linalg.norm(v1)
        tmp = np.cross(v1,v2)
        Zn = (tmp)/np.linalg.norm(tmp)
        Yn = np.cross(Xn, Zn)

        i = np.dot(Xn, v2)
        d = np.dot(Xn, v1)
        j = np.dot(Yn, v2)

        X = ((r1**2)-(r2**2)+(d**2))/(2*d)
        Y = (((r1**2)-(r3**2)+(i**2)+(j**2))/(2*j))-((i/j)*(X))
        Z1 = np.sqrt(max(0, r1**2-X**2-Y**2))
        Z2 = -Z1

        K1 = P1 + X * Xn + Y * Yn + Z1 * Zn
        K2 = P1 + X * Xn + Y * Yn + Z2 * Zn

        print("position 1 is",K1)
        print("position 2 is", K2)

        # dist = np.sqrt((K1[0]-P4[0])**2 + (K1[1]-P4[1])**2 + (K1[2]-P4[2])**2)
        # dist2 = np.sqrt((K2[0]-P4[0])**2 + (K2[1]-P4[1])**2 + (K2[2]-P4[2])**2)
        # print(dist)
        # print(dist2)

        # diff = np.array([abs(dist - r4), abs(dist2 - r4)])
        diff = np.array([math.dist(K1, targets[target,:]), math.dist(K2,
targets[target,:])])
```

```
            #print(diff)
            position_id = diff.argsort()[0]
            print(position_id)
            if position_id == 0:
                position = K1
            if position_id == 1:
                position = K2

            # print("Distance position 1 to 4th point is:",dist)
            # print("Distance position 2 to 4th point is:", dist2)
            # print("Measured distance to 4th point is:", r4)
            return position

        position = trilateration(P1, P2, P3, P4, d1, d2, d3, d4)
        error_x = position[0] - targets[target,0]
        error_y = position[1] - targets[target,1]
        error_z = position[2] - targets[target,2]
        positions.loc[target+1,['x']] = position[0]
        positions.loc[target+1,['y']] = position[1]
        positions.loc[target+1,['z']] = position[2]
        positions.loc[target+1,['error x']] = error_x
        positions.loc[target+1,['error y']] = error_y
        positions.loc[target+1,['error z']] = error_z

        RMS = math.dist(position, targets[target,:])
        positions.loc[target+1,['RMS']] = RMS
        print(position)
        print(RMS)

    with pd.ExcelWriter(excel_writer, mode = 'a', if_sheet_exists = 'replace') as writer:
        positions.to_excel(writer, sheet_name = 'depth_registration', index_label= 'Target')
```

Appendix D

Questionnaires cadaver study

Name:

Strongly disagree	Disagree	Neutral	Agree	Strongly agree
1	2	3	4	5

Experiment 1:

Landmark-based registration

Statement	**Score**
Registration was quick.	
Registration was easy to perform.	
Based on my own interpretation of the anatomy, the holographic overlay seemed accurate.	
I would use this registration method during surgery (pre-incision).	
Comments:	

Contour registration

Statement	**Score**
Registration was quick.	
Registration was easy to perform.	
Based on my own interpretation of the anatomy, the holographic overlay seemed accurate.	
I would use this registration method during surgery (pre-incision).	
Comments:	

ToF camera registration

Statement	**Score**
Registration was quick.	
Registration was easy to perform.	
Based on my own interpretation of the anatomy, the holographic overlay seemed accurate.	
I would use this registration method during surgery (pre-incision).	
Comments:	

Experiment 2:
N.B.: This questionnaire was completed for both surface matching methods

Pre-incision

Statement	**Score**
Based on palpation alone, I was confident about the localisation of the rib/tumour.	
Based on my own interpretation of the anatomy, the holographic overlay seemed accurate.	
The use of the HoloLens improved my confidence about localisation of the rib/tumour.	
I would dare to make surgical decisions based on the projection of the HoloLens.	
The use of the HoloLens changed my surgical plan.	
Comments:	

Post-incision

Statement	**Score**
Based on palpation/inspection alone, I was confident about the localisation of the rib/tumour.	
Based on my own interpretation of the anatomy, the holographic overlay seemed accurate.	
The use of the HoloLens improved my confidence about localisation of the rib/tumour.	
I would dare to make surgical decisions based on the projection of the HoloLens.	
The use of the HoloLens changed my surgical plan.	
I would use this registration method during surgery (post-incision).	
Comments:	

General:

Statement	**Score**
I see potential in the use of the HoloLens during chest wall resections.	
The HoloLens has added value in the localisation of the rib/tumour pre-incision.	
The HoloLens has added value in the localisation of the rib/tumour post-incision.	
The use of the HoloLens is worth the additional time and steps prior to surgery (selection of landmarks, CT scan in operative position etc.).	
The use of the HoloLens is worth the additional time and steps during surgery (time for registration, visualisation etc.).	

Appendix E

Additional figures Chapter 6

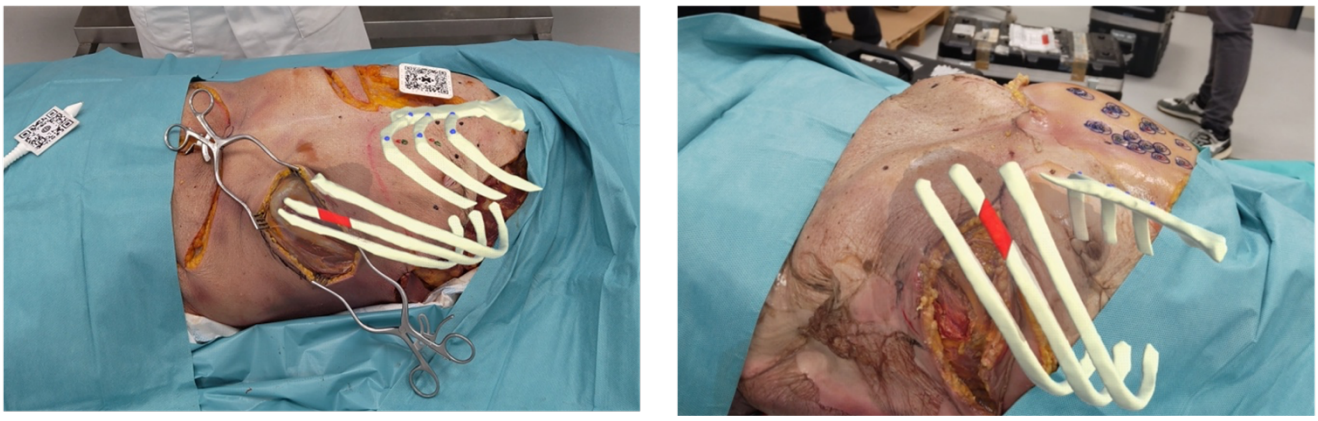

Figure 17. *Results of registration post-incision by use of the ToF camera registration method.*

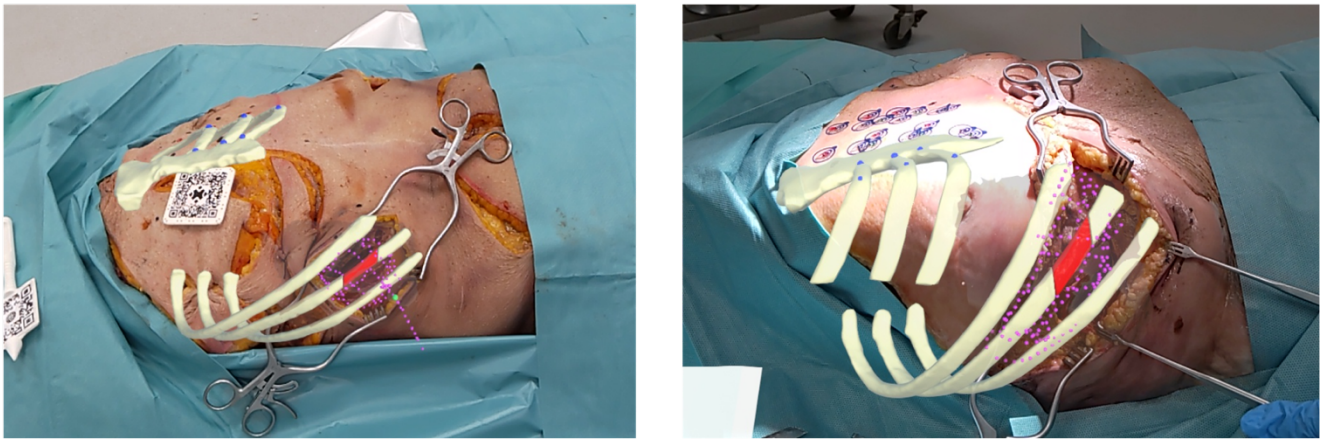

Figure 18. *Results of registration post-incision by use of the contour registration method.*